

On Hybrid Radar Fusion for Integrated Sensing and Communication

Akhileswar Chowdary Gaddam, Ahmad Bazzi, Marwa Chafii

Abstract—The following paper introduces a novel integrated sensing and communication (ISAC) scenario termed hybrid radar fusion. In this setting, the dual-functional radar and communications (DFRC) base station (BS) acts as a mono-static radar in the downlink (DL), for sensing purposes, while performing its DL communication tasks. Meanwhile, the communication users act as distributed bi-static radar nodes in the uplink (UL) following a frequency-division duplex protocol. The DFRC BS fuses the information available at different DL and UL resource bands to estimate the angles-of-arrival (AoAs) of the multiple targets existing in the scene. In this work, we derive the maximum likelihood (ML) criterion for the hybrid radar fusion problem at hand. Additionally, we design efficient estimators; the first algorithm is based on an alternating optimization approach to solve the ML criterion, while the second one designs an optimization framework that leads to an alternating subspace approach to estimate AoAs for both the target and users. Finally, we demonstrate the superior performance of both algorithms in different scenarios, and the gains offered by these proposed methods through numerical simulations.

Index Terms—Integrated Sensing and Communication (ISAC), Dual-Functional Radar and Communications (DFRC), radar fusion, hybrid radar, 6G

I. INTRODUCTION

Despite having numerous similarities in terms of signal processing and system design, radar sensing and wireless communication have been evolving individually for many years [1]. Interestingly, both radar and communication systems have quite a number of signal processing features that can be shared in common, thus favoring their joint design [2]–[8]. Indeed, integrated sensing and communication (ISAC) can open the way for ground-breaking applications, for example in the automotive sector [9], Internet of things (IoT), and robotics.

ISAC has been investigated for different scenarios and challenges, including non-orthogonal multiple access (NOMA) [10], [11], holographic communications [12], optical fiber [13], dual-functional radar and communication (DFRC) [14], intelligent reflecting surface (IRS) [15], waveform design [16], unmanned aerial vehicle (UAV) [17], beamforming design [18], IoT [19], just to name a few. Due to the interoperability

between the radar and communication sub-systems, ISAC has a variety of tangible benefits, such as spectrum efficiency [20], less expensive modem by unifying hardware and software resources across sensing and communication tasks [9]. These advantages bring a significant number of difficulties and research issues that must be resolved, such as the trade-offs between high communication rates and high-resolution sensing. One of the earliest appearances of ISAC was in the 60s [21], where communication and radar tasks share the same power, spectrum and resources. In particular, pulse interval modulation was used for radar pulses and communication was embedded in those pulses. Owing to advances in waveform design, beamforming, and software-defined radios (SDRs), ISAC has become a technological reality.

ISAC can be categorized into three main categories, from a design perspective. A *joint design* approach aims at developing new waveforms intended for both sensing and communications, while offering tradeoffs between different key performance indicators (KPIs), such as data rates, capacity, energy for communications and probability of detection and Cramér-Rao bound (CRB) for radar sensing. For example, the work in [22] proposes a joint design of communication and sensing waveforms with adjustable peak-to-average power ratio (PAPR), allowing trade-offs between radar performance, communication rate and PAPR. Moreover, another design is *radar-centric* ISAC, where a radar waveform is considered and communication information is inserted onto the radar waveform [23]–[27]. Finally, *communication-centric* ISAC takes a communication waveform, for example, orthogonal frequency-division multiplexing (OFDM) or orthogonal time frequency space (OTFS), and estimates sensing parameters based on channel information probed in that waveform. Here sensing is an “add-on”. The interested reader is referred to [28], [29] for communication-centric ISAC.

DFRC, a design technique for integrating ISAC tasks, simultaneously performs radar and communication functions using a common transmit/receive aperture [30]. For the radar counterpart, two common settings are mono-static [31] radar and bi-static [32] radar. In the former, the transmitting and receiving radar units are co-located so that the distance between the two units is negligible, relative to their distance toward the target. In the latter, both units are separated by a significant distance. Even more, two types of transmissions are common in radar, namely active and passive. In active radar [33], the radar exploits a known transmitted waveform in order to estimate the sensing parameters of the targets through the echo return signal. On the other hand, passive radar [34] allows the usage of remote transmitters, also called

Akhileswar Chowdary Gaddam is with the NYU Tandon School of Engineering, Brooklyn, 11201, NY, USA (email: ag8771@nyu.edu)

Ahmad Bazzi is with the Engineering Division, New York University (NYU) Abu Dhabi, 129188, UAE (email: ahmad.bazzi@nyu.edu).

Marwa Chafii is with Engineering Division, New York University (NYU) Abu Dhabi, 129188, UAE and NYU WIRELESS, NYU Tandon School of Engineering, Brooklyn, 11201, NY, USA (email: marwa.chafii@nyu.edu).

Manuscript received xxx

donors, in conjunction with active radars to make use of properties on different bands, without the knowledge of a particular waveform. Also, active/passive radar system [35] is also possible, where the target is seen as a passive illuminator and the active radar transmitter is operating on the co-channel within the same frequency band. In this paper, herein, we propose a new scheme named hybrid radar that considers both mono-static and bi-static settings, where the DFRC base station (BS) acts as a mono-static radar and the communication users act as distributed bi-static radars in the uplink (UL) following a frequency-division duplex (FDD) protocol.

A. Literature Review

To unbolt the potential of sensing capabilities in ISAC systems, various lines of research work have been conducted in the literature. In particular, the paper in [36] exploits OFDM based waveforms in the downlink (DL) only, from a mono-static radar perspective, and performs delay and doppler estimation via periodogram criterion, which is only optimal for a single target. In addition, the paper in [37] considers a bi-static setting, in which the sensing and communication tasks are performed in orthogonal sets of sub-carriers, where the sub-carriers allocated to sensing are distributed among antennas in an interleaved fashion. Besides, the paper in [38] proposes an ISAC multi-user IRS-aided scheme, capable of carrying out UL data communications, while simultaneously performing target localization. Moreover, OTFS [39], [40] for ISAC systems have been proposed in [41], where UL, as well as DL, communications are considered for vehicular communication systems. Their work has led to a novel model for delay-Doppler domain characterization for channel estimation. In the UL phase, the roadside unit (RSU) infers the delay-Doppler components associated with each path to form a map of the vehicular network. As for the DL, the RSU constructs beamformers based on the predicted sensing parameters. It should be noted that the joint exploitation of UL/DL data was not part of the framework. Nevertheless, [42] investigates multi-beam systems for ISAC for 5G-new radio (NR) using OFDM waveforms. The BS in this study is a mono-static one, and joint range and angle of arrival (AoA) estimation are modeled as sensing parameters, which further assists the beam-scanning procedure. However, the framework utilizes only the DL information, and therefore the UL information available from different communication users is neglected. Meanwhile, [18], [43] consider the joint design of beamforming for communication and sensing purposes, which is well-suited for beam-scanning applications. These frameworks also rely on DL-only communication information for sensing purposes. Furthermore, from a physical-layer security ISAC perspective, the work in [44] provides sensing estimation based on the eavesdropper location to improve the secrecy rate of the system. In short, the framework utilizes DL-only information for the radar echo. To the best of our knowledge, there does not exist any ISAC scheme in the literature that functions on a hybrid monostatic and bistatic mode and fuses UL and DL information to efficiently estimate target sensing parameters.

B. Contributions

In this paper, we propose a hybrid radar fusion system model, that combines both monostatic and bistatic modes, where the DFRC BS exploits the echos due to the DL communication signals, in conjunction with UL signals from a set of users associated with the DFRC BS. Each communication user transmits OFDM waveforms on its own resource band, where the DFRC BS then fuses the information from different resources to estimate angles of arrival (AoAs) of the targets in the scene. To this end, we summarize our contributions as follows

- **Hybrid Radar Model.** We coin the term *hybrid* because of the diverse and distributed radar functionality considered in this paper, i.e. the DL echo is associated with a mono-static radar setting, as the DFRC's transmit and receive units are assumed to be colocated. Meanwhile, a (user,DFRC) couple is seen as a bi-static radar, as the user is seen as a radar transmit unit in the UL, transmitting via an FDD protocol through OFDM communication signals, and the DFRC receive unit is the radar receiver. The DFRC's sophisticated task is to fuse the hybrid data at its disposal to estimate targets locations. *To the best of our knowledge, the estimation model that arises due to the hybrid nature appears in the literature for the first time.*
- **Fused Maximum Likelihood Criterion.** We derive the maximum likelihood (ML) criterion of the hybrid radar model, and highlight our interpretations, such as its resemblance with the classical ML criterion and the additional terms due to the participation of the communication users in the UL.
- **Fused and Efficient Estimators.** In light of the hybrid and dual nature of the available data, we propose two computationally attractive estimators. The first one explicitly tackles the ML criterion through an iterative optimization procedure that alternates between the target and user spaces. The second one is an iterative subspace estimator: inspired by the multiple signal classification (MUSIC) principle, we formulate novel optimization problems, which lead to a new iterative estimator that carefully projects and fuses target and user location estimates.
- **Extensive simulation results.** Various performance metrics evaluating sensing performance via OFDM communication waveforms are studied through simulations, demonstrating the effectiveness of utilizing fused data for the hybrid radar model. Numerical results show performance gains in terms of mean squared error (MSE) of the estimated AoAs for the targets, especially when more communication users participate in the UL.

C. Organization and Notations

The following paper is organized as follows. Section II introduces the hybrid radar fusion system model. Section III derives the ML criterion of the problem from a sensing perspective. Section IV designs an efficient fused ML estimator to estimate the AoAs of the different targets. Section V designs an optimization framework to derive a fused subspace

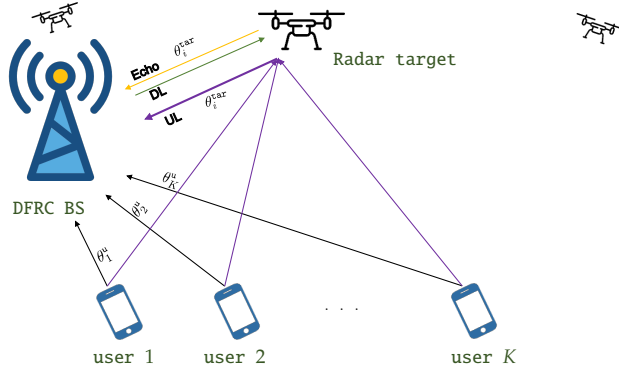


Fig. 1. The hybrid radar fusion system model comprised of a DFRC BS in mono-static mode listening to its DL echo, with K communication UL users and a radar target. Note that we only depict one target due to illustration purposes.

algorithm that iterates between user and target AoAs. Our simulation findings are illustrated and analyzed in Section VI. Section VII concludes the paper and gives future directions.

Notation: Upper-case and lower-case boldface letters denote matrices and vectors, respectively. $(\cdot)^T$, $(\cdot)^*$ and $(\cdot)^H$ represent the transpose, the conjugate and the transpose-conjugate operators. The empty set is \emptyset . The cardinality of set \mathcal{C} is $|\mathcal{C}|$. The set of all complex-valued $N \times M$ matrices is $\mathbb{C}^{N \times M}$. The determinant is $\det(\cdot)$. The trace is $\text{tr}(\cdot)$. The $N \times N$ identity matrix is \mathbf{I}_N . The projector operator onto the space spanned by the columns of matrix $\mathbf{A} \in \mathbb{C}^{N \times M}$ is \mathbf{P}_A and the corresponding orthogonal projector is $\mathbf{P}_A^\perp \triangleq \mathbf{I}_N - \mathbf{P}_A$. We index the $(i, j)^{\text{th}}$ element of matrix \mathbf{A} as $\mathbf{A}(i, j)$. The k^{th} column of \mathbf{A} is indexed as $\mathbf{A}(:, k)$. The span of \mathbf{A} , denoted by $\text{span}(\mathbf{A})$ returns the column space of \mathbf{A} . The Moore-Penrose pseudo-inverse of a matrix \mathbf{A} is \mathbf{A}^+ .

II. SYSTEM MODEL

Consider a DFRC BS transmitting OFDM symbols over its allocated band. In the DL, the ℓ^{th} transmitted OFDM signal can be expressed as

$$s_{0,\ell}(t) = \sum_{m \in \mathcal{C}_0} b_{m,0}^{(\ell)} \exp(j2\pi m \Delta_f t) \Pi(t - \ell T), \quad (1)$$

where \mathcal{C}_0 is the set of subcarriers corresponding to the allocated band in the DL. Furthermore, $b_{m,0}^{(\ell)}$ is the modulated symbol onto the m^{th} OFDM subcarrier within the ℓ^{th} OFDM symbol and Δ_f is the subcarrier spacing. It is also assumed that the downlink consists of L_0 OFDM symbols. Moreover, the OFDM symbol duration is given $T = \frac{1}{\Delta_f}$. Moreover, $\Pi(t)$ is a certain windowing function. The overall OFDM symbol duration is denoted as $T_o \triangleq T + T_{\text{CP}}$, where T_{CP} is the cyclic prefix duration. Assuming the ideal rectangular function, the window function should satisfy

$$\Pi(t) = \begin{cases} 1, & t \in [-T_{\text{CP}}, T] \\ 0, & \text{else,} \end{cases} \quad (2)$$

where T_{CP} should be greater than the maximum of propagation delays in order to guarantee a cyclic convolution with the channel.

The ℓ^{th} transmitted OFDM symbol from the single-antenna k^{th} communication user in the UL is given by

$$s_{k,\ell}(t) = \sum_{m \in \mathcal{C}_k} b_{m,k}^{(\ell)} \exp(j2\pi m \Delta_f t) \Pi(t - \ell T), \quad (3)$$

where \mathcal{C}_k is the set of subcarriers corresponding to the allocated band for the k^{th} communication user in the UL. Moreover, $b_{m,k}^{(\ell)}$ is the modulated symbol onto the m^{th} OFDM subcarrier by the k^{th} communication user within the ℓ^{th} OFDM symbol. Also, the transmission consists of L_k OFDM symbols for the k^{th} communication user. Note that $\mathcal{C}_0 \cap \mathcal{C}_1 \cap \dots \cap \mathcal{C}_K = \emptyset$ and $\mathcal{C}_0 \cup \mathcal{C}_1 \cup \dots \cup \mathcal{C}_K = \{0, 1, \dots, M-1\}$, where M is the total number of subcarriers occupied by the entire system, i.e. the total occupied bandwidth is $M\Delta_f$.

After downconversion, and assuming that the users are synchronized for sake of simplicity, the ℓ^{th} received OFDM symbol at the n^{th} receive antenna of the DFRC BS is given as

$$r_{n,\ell}(t) = r_{n,\ell}^{\text{echo}}(t) + \sum_{k=1}^K r_{n,\ell,k}^{\text{UL}}(t) + w_{n,\ell}(t), \quad (4)$$

where $r_{n,\ell}^{\text{echo}}(t)$ is the received echo signal due to the presence of the radar targets, i.e.

$$r_{n,\ell}^{\text{echo}}(t) = \sum_{i=1}^q \gamma_{i,\ell}^{\text{tar}} a_n(\theta_i^{\text{tar}}) s_{0,\ell}(t - 2\tau_i^{\text{tar}}), \quad (5)$$

where q is the number of targets present in the scene. Furthermore, $a_n(\theta)$ is the steering response of the n^{th} antenna due to a signal arriving at angle θ and $r_{n,\ell,k}^{\text{UL}}(t)$ is the received signal due to the channel between the k^{th} communication user and the DFRC BS, taking into account the direct line of sight (LoS) and the bounces due to the presence of targets, i.e.

$$r_{n,\ell,k}^{\text{UL}}(t) = \gamma_{0,\ell,k}^{\text{u}} a_n(\theta_k^{\text{u}}) s_{k,\ell}(t - \tau_k^{\text{u}}) + \sum_{i=1}^q \gamma_{i,\ell,k}^{\text{tar}} a_n(\theta_i^{\text{tar}}) s_{k,\ell}(t - \phi_{k,i}), \quad (6)$$

where $\gamma_{i,\ell}^{\text{tar}}$ is the complex channel gain between the DFRC BS and the i^{th} target on the ℓ^{th} OFDM symbol, which are proportional to the radar cross-section (RCS) of the targets. The AoA and time of arrival (ToA) between the DFRC BS and the i^{th} target are denoted as θ_i^{tar} and τ_i^{tar} , respectively. Moreover, the complex channel gain between the DFRC BS and the k^{th} communication user on the ℓ^{th} OFDM symbol is denoted as $\gamma_{0,\ell,k}^{\text{u}}$, whereas the overall complex channel gain between the k^{th} communication user towards the i^{th} target then towards the DFRC BS is denoted as $\gamma_{i,\ell,k}^{\text{tar}}$. Furthermore, the AoA and ToA between the k^{th} communication user and the DFRC BS are denoted as θ_k^{u} and τ_k^{u} , respectively. Additionally, the overall ToA traversing from the k^{th} communication user towards the i^{th} target, then towards the DFRC BS is denoted as $\phi_{k,i}$. The background noise in (4) is denoted as $w_{n,\ell}(t)$, which is assumed to be independently and identically distributed (i.i.d) additive white Gaussian noise (AWGN). Now, plugging equations (1) and (3) in equations (5) and (6), and sampling at regular intervals of $p \triangleq p \frac{T}{M}$, we can express equation (4) as follows

$$\begin{aligned}
 r_{n,\ell}[p] &= \sum_{i=1}^q \sum_{m \in \mathcal{C}_0} b_{m,0}^{(\ell)} \exp(j2\pi \frac{mp}{M}) c_m(2\tau_i^{\text{tar}}) \gamma_{i,\ell}^{\text{tar}} a_n(\theta_i^{\text{tar}}) \\
 &+ \sum_{k=1}^K \sum_{m \in \mathcal{C}_k} b_{m,k}^{(\ell)} \exp(j2\pi \frac{mp}{M}) c_m(\tau_k^{\text{u}}) \gamma_{0,\ell,k}^{\text{u}} a_n(\theta_k^{\text{u}}) \\
 &+ \sum_{k=1}^K \sum_{m \in \mathcal{C}_k} \sum_{i=1}^q b_{m,k}^{(\ell)} \exp(j2\pi \frac{mp}{M}) c_m(\phi_{k,i}) \gamma_{i,\ell,k}^{\text{tar}} a_n(\theta_i^{\text{tar}}) \\
 &+ w_{n,\ell}[p],
 \end{aligned} \tag{7}$$

where $c_m(\tau) = \exp(-j2\pi m \Delta_f \tau)$. Now, gathering M time samples of $r_{n,\ell}[p]$ and performing an M -point discrete Fourier transform (DFT), we have

$$R_{n,\ell,m} = \frac{1}{M} \sum_{p=0}^{M-1} r_{n,\ell}[p] \exp(-j2\pi \frac{mp}{M}). \tag{8}$$

Without loss of generality, we assume that the symbols $b_{m,k}^{(\ell)}$ are training symbols, which further allows equalization for channel estimation at the DFRC BS. This is accomplished as follows

$$Y_{n,\ell,m} = \frac{(b_{m,k}^{(\ell)})^*}{|b_{m,k}^{(\ell)}|^2} R_{n,\ell,m}, \quad k = 0 \dots K \tag{9}$$

Using equations (7) and (8) in (9), we get

$$Y_{n,\ell,m} = \sum_{i=1}^q c_m(2\tau_i^{\text{tar}}) \gamma_{i,\ell}^{\text{tar}} a_n(\theta_i^{\text{tar}}) + W_{n,\ell,m}, \tag{10}$$

for $m \in \mathcal{C}_0$, and

$$\begin{aligned}
 Y_{n,\ell,m} &= c_m(\tau_k^{\text{u}}) \gamma_{0,\ell,k}^{\text{u}} a_n(\theta_k^{\text{u}}) \\
 &+ \sum_{i=1}^q c_m(\phi_{k,i}) \gamma_{i,\ell,k}^{\text{tar}} a_n(\theta_i^{\text{tar}}) + W_{n,\ell,m},
 \end{aligned} \tag{11}$$

for $m \in \mathcal{C}_k$ for all $k = 1 \dots K$. Equations (10) and (11) can be rearranged, via matrix form, as follows,

$$\mathbf{Y}_0 = \mathbf{A}(\Theta^{\text{tar}}) \mathbf{X}_0 + \mathbf{W}_0, \tag{12}$$

$$\mathbf{Y}_k = [\mathbf{a}(\theta_k^{\text{u}}) \quad \mathbf{A}(\Theta^{\text{tar}})] \mathbf{X}_k + \mathbf{W}_k, \quad k = 1 \dots K \tag{13}$$

Let $\mathcal{C}_k = \{p_1, p_2, \dots, p_{|\mathcal{C}_k|}\}$ be the subcarrier indices occupied by the k^{th} communication user in the UL. To this extent, we can define \mathbf{X}_k as

$$\mathbf{X}_k = [\mathbf{x}_{1,p_1}^{(k)}, \dots, \mathbf{x}_{L_k,p_1}^{(k)}, \dots, \mathbf{x}_{1,p_{|\mathcal{C}_k|}}^{(k)}, \dots, \mathbf{x}_{L_k,p_{|\mathcal{C}_k|}}^{(k)}], \tag{14}$$

where $\mathbf{x}_{\ell,m}^{(k)}$ is a function of the gains and delays. Notice that $\mathbf{X}_k \in \mathbb{C}^{(q+1) \times \bar{L}_k}$ and $\bar{L}_k = L_k |\mathcal{C}_k|$ is the overall number of snapshots seen by the DFRC BS from the k^{th} communication user in the UL. Likewise, $\mathbf{X}_0 \in \mathbb{C}^{q \times \bar{L}_0}$ and \bar{L}_0 is the total number of snapshots seen through the transmitted DL OFDM frame. Furthermore, the manifold matrix $\mathbf{A}(\Theta^{\text{tar}})$ is given by

$$\mathbf{A}(\Theta^{\text{tar}}) = [\mathbf{a}(\theta_1^{\text{tar}}) \quad \dots \quad \mathbf{a}(\theta_q^{\text{tar}})] \in \mathbb{C}^{N \times q}, \tag{15}$$

and the steering vector is given by

$$\mathbf{a}(\theta) = [\mathbf{a}_1(\theta) \quad \dots \quad \mathbf{a}_N(\theta)]^T \in \mathbb{C}^{N \times 1}. \tag{16}$$

Moreover, the entries of \mathbf{W}_k contain $W_{n,\ell,m}$ for $m \in \mathcal{C}_k$. In this paper, since we are interested in target AoA estimation, we shall treat the entries of $\mathbf{X}_0, \mathbf{X}_1 \dots \mathbf{X}_K$ as nuisance parameters, as the estimation of complex channel gains and ToA parameters is not the main focus herein.

Furthermore, observing equations (12) and (13), one can directly relate each equation to the classical AoA estimation problem. However, we would like to stress the fundamental difference between the AoA problem at hand and the classical one. Even though each of the $K+1$ matrix equations in (12) and (13) are classical AoA-type equations, the information contained over all equations is not. More specifically, each communication user over its occupied bandwidth, defined by \mathcal{C}_k , contains the manifold of interest $\mathbf{A}(\Theta^{\text{tar}})$ appended by an additional unknown channel $\mathbf{a}(\theta_k^{\text{u}})$, linking the k^{th} communication user towards the DFRC BS.

Our system model is illustrated in Fig. 1. We can see that the DFRC BS broadcasts the DL communication data and listens to the received echo at its allocated band. Meanwhile, the users each transmit OFDM symbols within their own band in the UL. Each communication contributes in two components: (i) a LoS path between itself and the DFRC BS, which is assumed to be unknown and (ii) the bounce from the target towards the DFRC BS within the users allocated band. The DFRC BS would then fuse the information available at all the bands, in order to estimate the unknown AoAs.

Before we introduce the estimation criteria and methods, we would like to take a moment and observe the joint model appearing in equations (12) and (13). The joint consideration of the $K+1$ models is the first time to be addressed, from an estimation perspective. Indeed, if we regard each of the $K+1$ models separately, then we coincide with a classical AoA estimation problem. However, the fused processing of the $K+1$ models can be leveraged to our advantage, as a *common manifold* is shared across all the $K+1$ models, i.e. $\mathbf{A}(\Theta^{\text{tar}})$. To this end, we are ready to address our problem: by fusing the observations $\{\mathbf{Y}_0, \mathbf{Y}_1 \dots \mathbf{Y}_K\}$ as defined in (12) and (13), we would like to estimate Θ^{tar} , as well as Θ^{u} .

III. FUSED MAXIMUM LIKELIHOOD

In this section, we derive the deterministic ML for estimating Θ^{tar} and Θ^{u} . The deterministic ML regards the sample functions as unknown deterministic sequences, rather than random processes. As shall be clarified, we can interpret our ML criterion as a fused maximum likelihood (FML) one.

Denoting $\mathbf{Y} = [\mathbf{Y}_0 \quad \mathbf{Y}_1 \quad \dots \quad \mathbf{Y}_K]$, we can express the joint density function of the observed data per allocated bandwidth as follows

$$\begin{aligned}
 f(\mathbf{Y}) &= \prod_{k=0}^K \prod_{p=1}^{\bar{L}_k} \frac{1}{\pi \det(\sigma^2 \mathbf{I})} \\
 &\times \exp\left(-\frac{1}{\sigma^2} \|\mathbf{Y}_k(:,p) - \mathbf{A}_k \mathbf{X}_k(:,p)\|^2\right),
 \end{aligned} \tag{17}$$

where, for notation's sake, we denote

$$\mathbf{A}_k = \begin{cases} \mathbf{A}(\Theta^{\text{tar}}) & , k = 0 \\ [\mathbf{a}(\theta_k^{\text{u}}) \quad \mathbf{A}(\Theta^{\text{tar}})] & , 1 \leq k \leq K. \end{cases} \tag{18}$$

Note that $f(\mathbf{Y})$ is conditioned over $\mathbf{X}_0 \dots \mathbf{X}_K, \sigma^2, \boldsymbol{\Theta}^{\text{tar}}, \boldsymbol{\Theta}^{\text{u}}$, and this dependency has been omitted for sake of compact notation. Ignoring constant terms, the log-likelihood function can be expressed as

$$\begin{aligned} \mathcal{L} &\triangleq \log f(\mathbf{Y}) \\ &\sim -N\bar{L} \log \sigma^2 - \frac{1}{\sigma^2} \sum_{k=0}^K \sum_{p=1}^{\bar{L}_k} \|\mathbf{Y}_k(:, p) - \mathbf{A}_k \mathbf{X}_k(:, p)\|^2, \end{aligned} \quad (19)$$

where $\bar{L} = \sum_{k=0}^K \bar{L}_k$. The ML criterion is now given as

$$\left\{ \hat{\sigma}^2, \hat{\mathbf{X}}, \hat{\boldsymbol{\Theta}}^{\text{tar}}, \hat{\boldsymbol{\Theta}}^{\text{u}} \right\} = \arg \max_{\{\sigma^2, \mathbf{X}, \boldsymbol{\Theta}^{\text{tar}}, \boldsymbol{\Theta}^{\text{u}}\}} \mathcal{L} \quad (20)$$

where $\mathbf{X} = [\mathbf{X}_0 \ \mathbf{X}_1 \ \dots \ \mathbf{X}_K]$. To proceed, we first carry out the maximization process over σ^2 by fixing $\mathbf{X}, \boldsymbol{\Theta}^{\text{tar}}, \boldsymbol{\Theta}^{\text{u}}$. This gives us

$$\hat{\sigma}^2 = \frac{1}{N\bar{L}} \sum_{k=0}^K \sum_{p=1}^{\bar{L}_k} \|\mathbf{Y}_k(:, p) - \mathbf{A}_k \mathbf{X}_k(:, p)\|^2. \quad (21)$$

Replacing (21) back into the log-likelihood function and ignoring constant terms again, we get

$$-N\bar{L} \log \left(\frac{1}{N\bar{L}} \sum_{k=0}^K \sum_{p=1}^{\bar{L}_k} \|\mathbf{Y}_k(:, p) - \mathbf{A}_k \mathbf{X}_k(:, p)\|^2 \right). \quad (22)$$

Using the monotonic property of the log function, the optimization criterion in (22) is now

$$\left\{ \hat{\mathbf{X}}, \hat{\boldsymbol{\Theta}}^{\text{tar}}, \hat{\boldsymbol{\Theta}}^{\text{u}} \right\} = \arg \min_{\{\mathbf{X}, \boldsymbol{\Theta}^{\text{tar}}, \boldsymbol{\Theta}^{\text{u}}\}} \sum_{k=0}^K \sum_{p=1}^{\bar{L}_k} \|\mathbf{Y}_k(:, p) - \mathbf{A}_k \mathbf{X}_k(:, p)\|^2. \quad (23)$$

Now fixing $\boldsymbol{\Theta}^{\text{tar}}, \boldsymbol{\Theta}^{\text{u}}$, the optimization with respect of \mathbf{X}_k is the well known least squares (LS) over the associated communication user, i.e.

$$\hat{\mathbf{X}}_k = (\mathbf{A}_k^H \mathbf{A}_k)^{-1} \mathbf{A}_k^H \mathbf{Y}_k. \quad (24)$$

Plugging (24) into (23), we get

$$\left\{ \hat{\boldsymbol{\Theta}}^{\text{tar}}, \hat{\boldsymbol{\Theta}}^{\text{u}} \right\} = \arg \min_{\{\boldsymbol{\Theta}^{\text{tar}}, \boldsymbol{\Theta}^{\text{u}}\}} \sum_{k=0}^K \sum_{p=1}^{\bar{L}_k} \|\mathbf{Y}_k(:, p) - \mathbf{P}_k \mathbf{Y}_k(:, p)\|^2, \quad (25)$$

where \mathbf{P}_k is the projector matrix projecting onto the column space of matrix \mathbf{A}_k , namely

$$\mathbf{P}_k = \mathbf{A}_k (\mathbf{A}_k^H \mathbf{A}_k)^{-1} \mathbf{A}_k^H. \quad (26)$$

The criterion in (25) can be replaced as

$$\left\{ \hat{\boldsymbol{\Theta}}^{\text{tar}}, \hat{\boldsymbol{\Theta}}^{\text{u}} \right\} = \arg \max_{\{\boldsymbol{\Theta}^{\text{tar}}, \boldsymbol{\Theta}^{\text{u}}\}} \sum_{k=0}^K \sum_{p=1}^{\bar{L}_k} \|\mathbf{P}_k \mathbf{Y}_k(:, p)\|^2, \quad (27)$$

A more compact and convenient form to express the above ML cost is via the trace operator, i.e.

$$\left\{ \hat{\boldsymbol{\Theta}}^{\text{tar}}, \hat{\boldsymbol{\Theta}}^{\text{u}} \right\} = \arg \max_{\{\boldsymbol{\Theta}^{\text{tar}}, \boldsymbol{\Theta}^{\text{u}}\}} \sum_{k=0}^K \text{tr} \left(\mathbf{P}_k \hat{\mathbf{R}}_k \right), \quad (28)$$

where $\hat{\mathbf{R}}_k$ is the sample covariance matrix of \mathbf{Y}_k ,

$$\hat{\mathbf{R}}_k = \frac{1}{\bar{L}_k} \mathbf{Y}_k \mathbf{Y}_k^H. \quad (29)$$

We coin the term FML, as the ML criterion naturally fuses information on the different bands specified by $\{C_k\}_{k=0}^K$. It is worth noting that, although the different bands associated with communication users appear to be independent from an estimation viewpoint, this is not the case. Due to the fact that $\mathbf{A}_0, \mathbf{A}_1 \dots \mathbf{A}_K$ contain a common subspace $\mathbf{A}(\boldsymbol{\Theta}^{\text{tar}})$, the samples over different bands can, to some extent, aid the estimation quality of $\hat{\boldsymbol{\Theta}}^{\text{tar}}$, even though each band adds another unknown. In other words, the k^{th} communication user introduces an unknown θ_k^{u} within the samples collected from that user. To highlight this even further, we invoke the block-wise formula of the projector matrix [45], i.e.

$$\mathbf{P}_{[\mathbf{A}, \mathbf{B}]} = \mathbf{P}_{\mathbf{A}} + \mathbf{P}_{\mathbf{B}\mathbf{A}} = \mathbf{P}_{\mathbf{A}} + \mathbf{P}_{\mathbf{P}_{\mathbf{A}}^{\perp} \mathbf{B}}, \quad (30)$$

where $\mathbf{P}_{\mathbf{A}}^{\perp} = \mathbf{I}_N - \mathbf{P}_{\mathbf{A}}$. Furthermore, we can express \mathbf{P}_k in the FML cost as

$$\mathbf{P}_k = \begin{cases} \mathbf{P}_{\mathbf{A}(\boldsymbol{\Theta}^{\text{tar}})}, & k=0 \\ \mathbf{P}_{\mathbf{A}(\boldsymbol{\Theta}^{\text{tar}})} + \mathbf{P}_{\mathbf{P}_{\mathbf{A}(\boldsymbol{\Theta}^{\text{tar}})}^{\perp} \mathbf{a}(\theta_k^{\text{u}})}, & 1 \leq k \leq K \end{cases} \quad (31)$$

Finally, plugging (31) in the FML cost in (28) and using the additive property of the trace, we have the following

$$\left\{ \hat{\boldsymbol{\Theta}}^{\text{tar}}, \hat{\boldsymbol{\Theta}}^{\text{u}} \right\} = \arg \max_{\{\boldsymbol{\Theta}^{\text{tar}}, \boldsymbol{\Theta}^{\text{u}}\}} \left\{ \text{tr} \left(\mathbf{P}_{\mathbf{A}(\boldsymbol{\Theta}^{\text{tar}})} \hat{\mathbf{R}} \right) + \sum_{k=1}^K \frac{\mathbf{a}^H(\theta_k^{\text{u}}) \mathbf{P}_{\mathbf{A}(\boldsymbol{\Theta}^{\text{tar}})}^{\perp} \hat{\mathbf{R}}_k \mathbf{P}_{\mathbf{A}(\boldsymbol{\Theta}^{\text{tar}})}^{\perp} \mathbf{a}(\theta_k^{\text{u}})}{\mathbf{a}^H(\theta_k^{\text{u}}) \mathbf{P}_{\mathbf{A}(\boldsymbol{\Theta}^{\text{tar}})}^{\perp} \mathbf{a}(\theta_k^{\text{u}})} \right\}, \quad (32)$$

where $\hat{\mathbf{R}} = \sum_{k=0}^K \hat{\mathbf{R}}_k$ is the fused covariance matrix containing both UL and DL information. The FML maximization criterion in (32) has a nice interpretation. Even though the manifold changes across bands, due to the presence of communication users at unknown locations, the first term of the FML criterion consists of summing the entire data across all the bands. In other words, this term appears due to the *common manifold*, $\mathbf{A}(\boldsymbol{\Theta}^{\text{tar}})$, spanned by the columns of $\mathbf{A}(\boldsymbol{\Theta}^{\text{tar}})$. The first term also resembles the classical deterministic ML criterion of the classical AoA estimation problem. On the other hand, the second term appearing in (32) constitutes the contributions of the K communication users. The k^{th} term tells us that in order to estimate θ_k^{u} , one must null the contributions of the common manifold $\mathbf{A}(\boldsymbol{\Theta}^{\text{tar}})$ via the orthogonal projector $\mathbf{P}_{\mathbf{A}(\boldsymbol{\Theta}^{\text{tar}})}^{\perp}$, before performing a Bartlett-type search to estimate θ_k^{u} , i.e. $\arg \max_{\theta} \frac{\bar{\mathbf{a}}^H(\theta) \hat{\mathbf{R}}_k \bar{\mathbf{a}}(\theta)}{\|\bar{\mathbf{a}}(\theta)\|^2}$, where $\bar{\mathbf{a}}(\theta) = \mathbf{P}_{\mathbf{A}(\boldsymbol{\Theta}^{\text{tar}})}^{\perp} \mathbf{a}(\theta)$. Even more, there are no cross-terms appearing between any two distinct users, which further simplifies the optimization procedure as presented in the next section.

IV. FUSED MAXIMUM LIKELIHOOD ESTIMATION

In this section, we develop a method based on alternating projections to compute a FML estimate of parameters $\boldsymbol{\Theta}^{\text{tar}}$

and Θ^u . Indeed, the naive ML estimator would perform a brute force search, resulting in a joint $(q + K)$ -dimensional search, which is computationally exhaustive. As we shall show, we can transform this multi-dimensional search, by carefully alternating between the spaces spanned by the common manifold and that of the users, to a sequence of one-dimensional searches that alternate until convergence.

A. Initialization

In the initialization phase of the proposed method, we target optimization of the common manifold term, i.e. the first term in (32). Therefore, this phase seeks the following

$$\hat{\Theta}^{\text{tar}} = \arg \max_{\Theta} \text{tr} \left(\mathbf{P}_{\mathbf{A}(\Theta)} \hat{\mathbf{R}} \right). \quad (33)$$

Since this problem corresponds to the classical AoA problem, we can adopt the classical alternating projection algorithm described in [46] to obtain an initial estimate of $\hat{\Theta}^{\text{tar}}$, i.e. $\hat{\Theta}_{(0)}^{\text{tar}}$. However, even though our main interest lies in the target AoAs, this step alone does not suffice, as the resulting estimates $\hat{\Theta}_{(0)}^{\text{tar}}$ are biased to the presence of the communication users as per (32).

B. Phase 1: Updating User AoAs

At iteration number p , one has access to $\hat{\Theta}_{(p)}^{\text{tar}}$, which is the p^{th} estimate of the target AoAs. This step involves K independent 1-dimensional searches to obtain $\hat{\Theta}_{(p)}^u$, namely, the k^{th} element of $\hat{\Theta}_{(p)}^u$ is updated according to the following criterion

$$[\hat{\theta}_k^u]_{(p)} = \arg \max_{\theta} \frac{\mathbf{a}^H(\theta) \mathbf{P}_{\mathbf{A}(\hat{\Theta}_{(p)}^{\text{tar}})}^{\perp} \hat{\mathbf{R}}_k \mathbf{P}_{\mathbf{A}(\hat{\Theta}_{(p)}^{\text{tar}})}^{\perp} \mathbf{a}(\theta)}{\mathbf{a}^H(\theta) \mathbf{P}_{\mathbf{A}(\hat{\Theta}_{(p)}^{\text{tar}})}^{\perp} \mathbf{a}(\theta)}. \quad (34)$$

Since the maximization processes are independent, i.e. the maximization with respect to $\hat{\theta}_i^u$ does not depend on $\hat{\theta}_j^u$, the K searches can be implemented in parallel.

C. Phase 2: Updating Target AoAs

At iteration number p and after the completion of Phase 1, we shall use $\hat{\Theta}_{(p)}^{\text{tar}}$, as well as $\hat{\Theta}_{(p)}^u$, to update target AoAs and generate their updated estimates, namely $\hat{\Theta}_{(p+1)}^{\text{tar}}$. In an attempt to estimate the AoA of the m^{th} target, we rewrite (32) as follows

$$[\hat{\theta}_m^{\text{tar}}]_{(p+1)} = \arg \max_{\theta} \sum_{k=0}^K \frac{\mathbf{a}^H(\theta) \mathbf{P}_{\hat{\mathbf{A}}_{k,m}^{(p)}}^{\perp} \hat{\mathbf{R}}_k \mathbf{P}_{\hat{\mathbf{A}}_{k,m}^{(p)}}^{\perp} \mathbf{a}(\theta)}{\mathbf{a}^H(\theta) \mathbf{P}_{\hat{\mathbf{A}}_{k,m}^{(p)}}^{\perp} \mathbf{a}(\theta)}, \quad (35)$$

where terms that do not depend on θ_m^{tar} have been omitted, due to their non-involvement in the optimization of θ_m^{tar} . The projector matrix appearing in (35) is obtained by omitting the column corresponding to $\mathbf{a}(\theta_m^{\text{tar}})$ from the matrix \mathbf{A}_k to form

$\hat{\mathbf{A}}_{k,m}^{(p)}$, then projecting to form $\mathbf{P}_{\hat{\mathbf{A}}_{k,m}^{(p)}}^{\perp}$. In other words, $\hat{\mathbf{A}}_{k,m}^{(p)}$ resembles the following form

$$\hat{\mathbf{A}}_{k,m}^{(p)} = \begin{cases} \mathbf{A}(\hat{\Theta}_{(p),m}^{\text{tar}}) & , k = 0 \\ \begin{bmatrix} \mathbf{a}(\hat{\theta}_k^u) & \mathbf{A}(\hat{\Theta}_{(p),m}^{\text{tar}}) \end{bmatrix} & , 1 \leq k \leq K, \end{cases} \quad (36)$$

and

$$\hat{\Theta}_{(p),m}^{\text{tar}} = [[\hat{\theta}_1^{\text{tar}}]_{(p+1)}, \dots, [\hat{\theta}_{m-1}^{\text{tar}}]_{(p+1)}, [\hat{\theta}_{m+1}^{\text{tar}}]_{(p)}, \dots, [\hat{\theta}_q^{\text{tar}}]_{(p)}] \quad (37)$$

After iterating through all target AoAs, we go back to phase 1 so that the method iterates between both phases. To this end, we summarize the proposed method in **Algorithm 1**. It is worth noting that a modified version of this method can be used, when one has prior knowledge of $\hat{\Theta}^u$ (or at least an estimate of it). This is simply achieved via bypassing phase one of **Algorithm 1**, and directly utilizing the given $\hat{\Theta}^u$ in phase two, i.e. using $\hat{\Theta}^u$ in (36) in order to estimate the target AoAs. This modification is of interest when users are assumed to be static, for example, an office environment or even static anchors providing regular communication signals towards the BS.

Algorithm 1 Efficient FML estimation

INPUT: $\hat{\mathbf{R}}_0 \dots \hat{\mathbf{R}}_K$

INITIALIZE:

Compute the fused covariance matrix, $\hat{\mathbf{R}} = \sum_{k=0}^K \hat{\mathbf{R}}_k$.

Run classical alternating projection method [46] to maximize first term of FML criterion in (32), as described in (33).

$p \leftarrow 0$

DO

PHASE 1: Updating User AoAs

 PARFOR $k = 1 \dots K$

 Update $[\hat{\theta}_k^u]_{(p)}$ via (34).

PHASE 2: Updating Target AoAs

 FOR $m = 1 \dots q$

 Form $\hat{\mathbf{A}}_{k,m}^{(p)}$ for all k as described in (36).

 Update $[\hat{\theta}_m^{\text{tar}}]_{(p+1)}$ via (35).

$p \leftarrow p + 1$

UNTIL $\|\hat{\Theta}_{(p+1)}^{\text{tar}} - \hat{\Theta}_{(p)}^{\text{tar}}\| + \|\hat{\Theta}_{(p+1)}^u - \hat{\Theta}_{(p)}^u\| < \epsilon$

return $\hat{\Theta}_{(p+1)}^{\text{tar}}, \hat{\Theta}_{(p+1)}^u$

V. FUSED SUBSPACE ESTIMATION

In this section, we introduce a novel method tailored to the hybrid radar fusion problem at hand. It is known that subspace-based methods are sub-optimal and require less computational complexity than maximum likelihood based ones. First, we revise the principle of MUSIC subspace estimation, then we take a step further to formulate an optimization framework inspired by the MUSIC principle, via subspace orthogonality tailored for the hybrid radar fusion problem.

A. Classical MUSIC estimation

We start by writing down the expression of the true covariance matrix corresponding to the model given in (12) and (13). Indeed, we have

$$\mathbf{R}_k \triangleq \mathbb{E}(\mathbf{Y}_k \mathbf{Y}_k^H) = \mathbf{A}_k \mathbf{R}_{xx}^{(k)} \mathbf{A}_k^H + \mathbf{R}_{ww,k}, \quad (38)$$

where \mathbf{A}_k is defined in (18), the covariance matrix $\mathbf{R}_{xx}^{(k)}$ is given as $\mathbf{R}_{xx}^{(k)} = \mathbb{E}(\mathbf{X}_k \mathbf{X}_k^H)$, and the covariance matrix $\mathbf{R}_{ww,k}$ is the covariance matrix of the AWGN which is assumed to be white over different frequency bands, i.e. $\mathbf{R}_{ww,k} = \sigma^2 \mathbf{I}_N$. To this end, the MUSIC principle relies on the observation that $\text{span}(\mathbf{A}_k) = \text{span}(\mathbf{R}_k)$, for noiseless scenarios. In fact, when noise is present, we can parametrize the eigenvalue decomposition (EVD) of \mathbf{R}_k as follows

$$\mathbf{R}_k = [\mathbf{U}_{S,k} \quad \mathbf{U}_{N,k}] \begin{bmatrix} \mathbf{\Lambda}_{S,k} & \mathbf{0} \\ \mathbf{0} & \mathbf{\Lambda}_{N,k} \end{bmatrix} [\mathbf{U}_{S,k} \quad \mathbf{U}_{N,k}]^H. \quad (39)$$

The matrices $\mathbf{U}_{S,k}$ and $\mathbf{U}_{N,k}$ are known to be the *signal* and *noise* subspaces on the k^{th} frequency band, respectively. The dimensions of $\mathbf{U}_{S,k}$ are the same as that of \mathbf{A}_k , and consequently, $\mathbf{U}_{N,k}$ would represent an orthogonal complement of $\mathbf{U}_{S,k}$. As a result, the eigenvalues are also decomposed into signal and noise eigenvalues contained in the diagonal block matrices $\mathbf{\Lambda}_{S,k}$ and $\mathbf{\Lambda}_{N,k}$, respectively. Indeed, given that $\mathbf{R}_{xx}^{(k)}$ is full-rank, the eigenvalues contained in the i^{th} diagonal entry of $\mathbf{\Lambda}_{S,k}$ is $\mathbf{\Lambda}_{S,k}(i, i) = \lambda_{k,i} + \sigma^2$, where $\lambda_{k,i}$ is the i^{th} largest eigenvalue of $\mathbf{A}_k \mathbf{R}_{xx}^{(k)} \mathbf{A}_k^H$. Moreover, it is easily verified that $\mathbf{\Lambda}_{N,k}(i, i) = \sigma^2$. This "jump" in eigenvalues aid in counting the number of signals within \mathbf{A}_k . Next, since $\text{span}(\mathbf{U}_{S,k}) = \text{span}(\mathbf{A}_k)$, we have that $\text{span}(\mathbf{U}_{N,k}) \perp \text{span}(\mathbf{A}_k)$. Therefore, we can guarantee perfect orthogonality between the steering vectors looking towards the true AoAs and the noise subspace, i.e. $\mathbf{A}_k^H \mathbf{U}_{N,k} = \mathbf{0}$, or equivalently $\|\mathbf{a}^H(\theta) \mathbf{U}_{N,k}\|^2 = 0$, for all $\theta \in [\theta_k^u, \boldsymbol{\Theta}^{\text{tar}}]$ if $1 \leq k \leq K$ and for all $\theta \in [\boldsymbol{\Theta}^{\text{tar}}]$ if $k = 0$. In practical scenarios, the expectation in (38) is replaced with a sample average, as dictated by (29). Therefore, the EVD operation is directly applied to the sample covariance matrix as follows

$$\widehat{\mathbf{R}}_k = [\widehat{\mathbf{U}}_{S,k} \quad \widehat{\mathbf{U}}_{N,k}] \begin{bmatrix} \widehat{\mathbf{\Lambda}}_{S,k} & \mathbf{0} \\ \mathbf{0} & \widehat{\mathbf{\Lambda}}_{N,k} \end{bmatrix} [\widehat{\mathbf{U}}_{S,k} \quad \widehat{\mathbf{U}}_{N,k}]^H. \quad (40)$$

Finally, the MUSIC criterion estimates the AoAs through peak finding of the following cost function

$$f(\theta) = \frac{1}{\|\mathbf{a}^H(\theta) \widehat{\mathbf{U}}_{N,k}\|_F^2}, \quad (41)$$

which turns out to be the MUSIC estimator, and the peaks of $f(\theta)$ correspond to the MUSIC estimates of $[\theta_k^u, \boldsymbol{\Theta}^{\text{tar}}]$.

B. Proposed Fused MUSIC Alternating Projection

In fact, from an optimization perspective [47], the MUSIC criterion can be cast as follows

$$(\mathcal{P}_{\text{MU}}) : \begin{cases} \min_{\omega_k(\theta)} & \|\omega_k(\theta) - \mathbf{a}(\theta)\|^2 \\ \text{s.t.} & \omega_k^H(\theta) \widehat{\mathbf{U}}_{N,k} = \mathbf{0}. \end{cases} \quad (42)$$

The solution of (42) is easily verified to be $\omega_k^{\text{MU}}(\theta) = \widehat{\mathbf{U}}_{S,k} \widehat{\mathbf{U}}_{S,k}^H \mathbf{a}(\theta)$, which when plugged back in the cost function of problem $(\mathcal{P}_{\text{MU}})$ gives us the MUSIC criterion in (41). In this section, we introduce a fused MUSIC approach based on alternating projections. The method is iterative by nature and alternates between user and target AoAs in a careful manner. In the first phase of the proposed fused method, we leverage the common manifold $\mathbf{A}(\boldsymbol{\Theta}^{\text{tar}})$ appearing solely in the DL. Via this common manifold, we first aim at obtaining a set of basis, where each spans the subspaces defined by $\mathbf{a}(\theta_1^u) \dots \mathbf{a}(\theta_K^u)$. Defining $\bar{\mathbf{R}}_k \triangleq \mathbf{P}_0^\perp \mathbf{R}_k$ for all k , where \mathbf{P}_0^\perp projects onto the nullspace of the common manifold $\mathbf{A}(\boldsymbol{\Theta}^{\text{tar}})$, i.e. $\mathbf{P}_0^\perp \mathbf{A}(\boldsymbol{\Theta}^{\text{tar}}) = \mathbf{0}$. This orthogonal projector will aid in nulling the effect of the targets, while focusing on the user ones. Assuming a diagonal matrix $\mathbf{R}_{xx}^{(k)}$, we have

$$\bar{\mathbf{R}}_k = r_{1,1}^{(k)} \mathbf{P}_0^\perp \mathbf{a}(\theta_k^u) \mathbf{a}^H(\theta_k^u) + \sigma^2 \mathbf{P}_0^\perp = \mathbf{U} \boldsymbol{\Sigma} \begin{bmatrix} \mathbf{v}_{S,k} & \tilde{\mathbf{V}}_{S,k} \end{bmatrix}, \quad (43)$$

where $r_{1,1}^{(k)}$ is the first element on the diagonal part of $\mathbf{R}_{xx}^{(k)}$. Now, applying singular value decomposition (SVD) on $\mathbf{P}_0^\perp \mathbf{R}_k$, as shown in the second equality, we can extract the singular vector spanning the only remaining vector $\mathbf{a}(\theta_k^u)$ by extracting the left singular vector corresponding to the strongest singular value within $\boldsymbol{\Sigma}$. Note that an estimate of \mathbf{P}_0^\perp can be obtained as follows

$$\widehat{\mathbf{P}}_0^\perp = \mathbf{I}_N - \widehat{\mathbf{U}}_{N,0} \widehat{\mathbf{U}}_{N,0}^H, \quad (44)$$

and, hence, an estimate of $\bar{\mathbf{R}}_k$ is obtained as

$$\widehat{\bar{\mathbf{R}}}_k = \widehat{\mathbf{P}}_0^\perp \widehat{\mathbf{R}}_k. \quad (45)$$

Now that we have $\mathbf{v}_{S,k}$, we can define an optimization problem tailored to extract the AoA of different communication users. To this end, we propose the following

$$(\mathcal{P}_k) : \begin{cases} \min_{\omega_k(\theta)} & \|\mathbf{v}_{S,k} \omega_k(\theta) - \mathbf{a}(\theta)\|^2 \\ \text{s.t.} & (\mathbf{v}_{S,k} \omega_k(\theta) - \mathbf{a}(\theta))^H \mathbf{P}_0^\perp = \mathbf{0}. \end{cases} \quad (46)$$

The above optimization problem adjusts $\omega_k(\theta)$ so that $\mathbf{v}_{S,k} \omega_k(\theta)$ matches the steering vector $\mathbf{a}(\theta)$ in all directions θ only for vectors residing in the orthogonal complement of $\mathbf{A}(\boldsymbol{\Theta}^{\text{tar}})$. More specifically, we seek to minimize the residual $\mathbf{v}_{S,k} \omega_k(\theta) - \mathbf{a}(\theta)$ for those lying in the orthogonal complement, \mathbf{P}_0^\perp . Accordingly, the associated Lagrangian function of the above optimization problem is given as

$$\mathcal{L}(\omega_k(\theta), \boldsymbol{\lambda}) = \|\mathbf{v}_{S,k} \omega_k(\theta) - \mathbf{a}(\theta)\|^2 - \left(\mathbf{v}_{S,k} \omega_k(\theta) - \mathbf{a}(\theta) \right)^H \mathbf{P}_0^\perp \boldsymbol{\lambda}^{\text{opt}}. \quad (47)$$

Deriving (47) with respect to $\omega_k(\theta)$, we get

$$\frac{\partial \mathcal{L}(\omega_k(\theta), \boldsymbol{\lambda})}{\partial \omega_k(\theta)} = 2\mathbf{v}_{S,k}^H \left(\mathbf{v}_{S,k} \omega_k(\theta) - \mathbf{a}(\theta) \right) - \mathbf{v}_{S,k}^H \mathbf{P}_0^\perp \boldsymbol{\lambda}. \quad (48)$$

Setting the above gradient to zero and using the property $\mathbf{v}_{S,k}^H \mathbf{v}_{S,k} = \mathbf{I}_N \forall k$, one gets a closed form in $\omega_k(\theta)$ as follows

$$\omega_k^{\text{opt}}(\theta) = \mathbf{v}_{S,k}^H \mathbf{a}(\theta) + \frac{1}{2} \mathbf{v}_{S,k}^H \mathbf{P}_0^\perp \boldsymbol{\lambda}^{\text{opt}}. \quad (49)$$

In order to obtain the optimal value of the Lagrangian multiplier $\boldsymbol{\lambda}^{\text{opt}}$, we derive the Lagrangian with respect to $\boldsymbol{\lambda}$ yielding the following first order conditions

$$\mathbf{P}_0^\perp \left(\mathbf{v}_{S,k} \mathbf{v}_{S,k}^H \mathbf{a}(\theta) + \frac{1}{2} \mathbf{v}_{S,k} \mathbf{v}_{S,k}^H \mathbf{P}_0^\perp \boldsymbol{\lambda}^{\text{opt}} - \mathbf{a}(\theta) \right) = \mathbf{0}. \quad (50)$$

Expanding, then re-arranging, we get

$$\boldsymbol{\lambda}^{\text{opt}} = 2(\mathbf{P}_0^\perp \mathbf{v}_{S,k} \mathbf{v}_{S,k}^H \mathbf{P}_0^\perp)^\dagger \mathbf{P}_0^\perp (\mathbf{I}_N - \mathbf{v}_{S,k} \mathbf{v}_{S,k}^H) \mathbf{a}(\theta). \quad (51)$$

Plugging equation (51) in (49)

$$\begin{aligned} \omega_k^{\text{opt}}(\theta) &= \mathbf{v}_{S,k}^H \mathbf{a}(\theta) \\ &+ \mathbf{v}_{S,k}^H \mathbf{P}_0^\perp (\mathbf{P}_0^\perp \mathbf{v}_{S,k} \mathbf{v}_{S,k}^H \mathbf{P}_0^\perp)^\dagger \mathbf{P}_0^\perp (\mathbf{I}_N - \mathbf{v}_{S,k} \mathbf{v}_{S,k}^H) \mathbf{a}(\theta). \end{aligned} \quad (52)$$

Using the property $\mathbf{Z}^T (\mathbf{Z}\mathbf{Z}^T)^\dagger = \mathbf{Z}^\dagger$ [48], we can rewrite (52) as

$$\omega_k^{\text{opt}}(\theta) = \mathbf{v}_{S,k}^H \mathbf{a}(\theta) + (\mathbf{P}_0^\perp \mathbf{v}_{S,k})^\dagger \mathbf{P}_0^\perp (\mathbf{I}_N - \mathbf{v}_{S,k} \mathbf{v}_{S,k}^H) \mathbf{a}(\theta). \quad (53)$$

which, after expanding and by definition of the Moore-Penrose pseudo-inverse, gives

$$\begin{aligned} \omega_k^{\text{opt}}(\theta) &= \mathbf{v}_{S,k}^H \mathbf{a}(\theta) + (\mathbf{P}_0^\perp \mathbf{v}_{S,k})^\dagger \mathbf{P}_0^\perp \mathbf{a}(\theta) \\ &- (\mathbf{P}_0^\perp \mathbf{v}_{S,k})^\dagger \mathbf{P}_0^\perp \mathbf{v}_{S,k} \mathbf{v}_{S,k}^H \mathbf{a}(\theta) \\ &= (\mathbf{P}_0^\perp \mathbf{v}_{S,k})^\dagger \mathbf{P}_0^\perp \mathbf{a}(\theta). \end{aligned} \quad (54)$$

Finally, plugging (54) in the cost function of problem (46), we get

$$g_k(\theta) = \left\| [\mathbf{v}_{S,k} (\mathbf{P}_0^\perp \mathbf{v}_{S,k})^\dagger \mathbf{P}_0^\perp - \mathbf{I}_N] \mathbf{a}(\theta) \right\|^2, \quad (55)$$

which can also be expressed as

$$g_k(\theta) = \left\| [\mathbf{v}_{S,k} (\mathbf{v}_{S,k}^H \mathbf{P}_0^\perp \mathbf{v}_{S,k})^{-1} \mathbf{v}_{S,k}^H \mathbf{P}_0^\perp - \mathbf{I}_N] \mathbf{a}(\theta) \right\|^2. \quad (56)$$

Now, we can get an estimate of $\hat{\theta}_k^{\text{u}}$, which is obtained through computing the maximum of $g_k^{-1}(\theta)$. The second phase entails in forming K orthogonal projectors $\hat{\mathbf{Q}}_1^\perp \dots \hat{\mathbf{Q}}_K^\perp$ as follows

$$\hat{\mathbf{Q}}_k^\perp = \mathbf{I}_N - \frac{1}{\|\mathbf{a}(\hat{\theta}_k^{\text{u}})\|^2} \mathbf{a}(\hat{\theta}_k^{\text{u}}) \mathbf{a}^H(\hat{\theta}_k^{\text{u}}), \quad \forall k = 1 \dots K \quad (57)$$

Next, we define K covariance matrices projected onto $\hat{\mathbf{Q}}_1^\perp \dots \hat{\mathbf{Q}}_K^\perp$, respectively, through $\mathbf{S}_k = \hat{\mathbf{Q}}_k^\perp \mathbf{R}_k$ for all $k \geq 1$. An estimate of \mathbf{S}_k is obtained as

$$\hat{\mathbf{S}}_k = \hat{\mathbf{Q}}_k^\perp \hat{\mathbf{R}}_k. \quad (58)$$

Using the same process as in the first phase, we can extract an estimate of the subspace spanned by the common manifold $\mathbf{A}(\boldsymbol{\Theta}^{\text{tar}})$ via the strongest q left singular vectors of $\hat{\mathbf{S}}_k$ as follows

$$\hat{\mathbf{S}}_k = \mathbf{U}_k \boldsymbol{\Sigma}_k \begin{bmatrix} \hat{\mathbf{V}}_{S,k} & \tilde{\mathbf{V}}_{S,k} \end{bmatrix}, \quad (59)$$

where $\hat{\mathbf{V}}_{S,k} \in \mathbb{C}^{N \times q}$ and $\text{span}(\mathbf{V}_{S,k}) = \text{span}(\mathbf{A}(\boldsymbol{\Theta}^{\text{tar}}))$ for all $k = 1 \dots K$. Prior to introducing the optimization problem that aims at estimating $\boldsymbol{\Theta}^{\text{tar}}$, it is worth noting that all the extracted singular vectors are mere estimates of the span of the common manifold, and so, it is crucial to fuse all the

estimated subspaces we have obtained into one optimization problem. For this, we propose problem (\mathcal{F}) given as follows

$$(\mathcal{F}) : \begin{cases} \min_{\{\boldsymbol{\omega}_k(\theta)\}_{k=0}^K} & \|\boldsymbol{\omega}_0(\theta) - \mathbf{a}(\theta)\|^2 \\ & + \sum_{k=1}^K \|\hat{\mathbf{V}}_{S,k} \boldsymbol{\omega}_k(\theta) - \mathbf{a}(\theta)\|^2 \\ \text{s.t.} & \boldsymbol{\omega}_0^H(\theta) \hat{\mathbf{U}}_{N,0} = \mathbf{0} \\ & (\hat{\mathbf{V}}_{S,k} \boldsymbol{\omega}_k(\theta) - \mathbf{a}(\theta))^H \hat{\mathbf{Q}}_k^\perp = \mathbf{0}, \forall k \geq 1. \end{cases} \quad (60)$$

We highlight two main aspects of problem (\mathcal{F}) defined in (60). The first one consists a simple MUSIC criterion in which we aim at fitting a direction vector $\boldsymbol{\omega}_0(\theta)$ orthogonal to $\hat{\mathbf{U}}_{N,0}$. The second one entails a joint subspace fit of all $\hat{\mathbf{V}}_{S,k}$ matrices through finding variable weight coefficients $\boldsymbol{\omega}_k(\theta)$ per direction θ that fits the steering vector in the same direction θ . However, to limit the search space to directions of interest, i.e. those not including the AoAs of the users, we constraint each residual to be orthogonal to $\hat{\mathbf{Q}}_k^\perp$. The Lagrangian associated with problem (\mathcal{F}) is given as

$$\begin{aligned} \mathcal{L} &= \|\boldsymbol{\omega}_0(\theta) - \mathbf{a}(\theta)\|^2 + \sum_{k=1}^K \|\hat{\mathbf{V}}_{S,k} \boldsymbol{\omega}_k(\theta) - \mathbf{a}(\theta)\|^2 \\ &- \boldsymbol{\omega}_0^H(\theta) \hat{\mathbf{U}}_{N,0} \boldsymbol{\lambda}_0 - \sum_{k=1}^K (\hat{\mathbf{V}}_{S,k} \boldsymbol{\omega}_k(\theta) - \mathbf{a}(\theta))^H \hat{\mathbf{Q}}_k^\perp \boldsymbol{\lambda}_k. \end{aligned} \quad (61)$$

The gradients with respect to $\boldsymbol{\omega}_0(\theta), \boldsymbol{\omega}_1(\theta) \dots \boldsymbol{\omega}_K(\theta)$ are given as

$$\frac{\partial \mathcal{L}}{\partial \boldsymbol{\omega}_0(\theta)} = 2(\boldsymbol{\omega}_0(\theta) - \mathbf{a}(\theta)) - \hat{\mathbf{U}}_{N,0} \boldsymbol{\lambda}_0, \quad (62)$$

$$\frac{\partial \mathcal{L}}{\partial \boldsymbol{\omega}_k(\theta)} = 2\hat{\mathbf{V}}_{S,k}^H (\hat{\mathbf{V}}_{S,k} \boldsymbol{\omega}_k(\theta) - \mathbf{a}(\theta)) - \hat{\mathbf{V}}_{S,k}^H \hat{\mathbf{Q}}_k^\perp \boldsymbol{\lambda}_k. \quad (63)$$

Setting the gradients to zero, we get the optimal values as

$$\boldsymbol{\omega}_0^{\text{opt}}(\theta) = \mathbf{a}(\theta) + \frac{1}{2} \hat{\mathbf{U}}_{N,0} \boldsymbol{\lambda}_0^{\text{opt}}, \quad (64)$$

$$\boldsymbol{\omega}_k^{\text{opt}}(\theta) = \hat{\mathbf{V}}_{S,k}^H \mathbf{a}(\theta) + \frac{1}{2} \hat{\mathbf{V}}_{S,k}^H \hat{\mathbf{Q}}_k^\perp \boldsymbol{\lambda}_k^{\text{opt}}. \quad (65)$$

Next, we derive the Lagrangian function with respect to the Lagrangian multipliers $\boldsymbol{\lambda}_0, \boldsymbol{\lambda}_1 \dots \boldsymbol{\lambda}_K$, and by setting them to zero at the optimal values, we get

$$\frac{\partial \mathcal{L}}{\partial \boldsymbol{\lambda}_0} = \hat{\mathbf{U}}_{N,0}^H \boldsymbol{\omega}_0^{\text{opt}}(\theta) = \mathbf{0}, \quad (66)$$

$$\frac{\partial \mathcal{L}}{\partial \boldsymbol{\lambda}_k} = \hat{\mathbf{Q}}_k^\perp (\hat{\mathbf{V}}_{S,k} \boldsymbol{\omega}_k^{\text{opt}}(\theta) - \mathbf{a}(\theta)) = \mathbf{0}, \forall k \geq 1. \quad (67)$$

Plugging equations (64) and (65) in equations (66) and (67), respectively, we get

$$\boldsymbol{\lambda}_0^{\text{opt}} = -2\hat{\mathbf{U}}_{N,0}^H \mathbf{a}(\theta), \quad (68)$$

$$\boldsymbol{\lambda}_k^{\text{opt}} = 2(\hat{\mathbf{Q}}_k^\perp \hat{\mathbf{V}}_{S,k} \hat{\mathbf{V}}_{S,k}^H \hat{\mathbf{Q}}_k^\perp)^\dagger \hat{\mathbf{Q}}_k^\perp (\mathbf{I}_N - \hat{\mathbf{V}}_{S,k} \hat{\mathbf{V}}_{S,k}^H) \mathbf{a}(\theta). \quad (69)$$

First, we replace $\boldsymbol{\lambda}_0^{\text{opt}}$ found in (68) back in (64) to get

$$\boldsymbol{\omega}_0^{\text{opt}}(\theta) = \mathbf{a}(\theta) - \hat{\mathbf{U}}_{N,0} \hat{\mathbf{U}}_{N,0}^H \mathbf{a}(\theta). \quad (70)$$

Then, we follow similar steps as those in equations (52),(53),(54) to get

$$\boldsymbol{\omega}_k^{\text{opt}}(\theta) = (\widehat{\mathbf{Q}}_k^\perp \widehat{\mathbf{V}}_{S,k}) + \widehat{\mathbf{Q}}_k^\perp \mathbf{a}(\theta), \quad \forall k = 1 \dots K. \quad (71)$$

Furthermore, we replace the quantities $\boldsymbol{\omega}_0^{\text{opt}}, \boldsymbol{\omega}_1^{\text{opt}} \dots \boldsymbol{\omega}_K^{\text{opt}}$ in the cost function of problem (60). Therefore, estimating the $\boldsymbol{\Theta}^{\text{tar}}$ involves a peak finding criterion of q AoAs through the following 1D search

$$\widehat{\boldsymbol{\Theta}}^{\text{tar}} = \arg \max_{\theta} h^{-1}(\theta), \quad (72)$$

where $h(\theta)$ is given by

$$h(\theta) = \|\widehat{\mathbf{U}}_{N,0}^H \mathbf{a}(\theta)\|^2 + \sum_{k=1}^K \|\widehat{\mathbf{V}}_{S,k} (\widehat{\mathbf{Q}}_k^\perp \widehat{\mathbf{V}}_{S,k}) + \widehat{\mathbf{Q}}_k^\perp \mathbf{a}(\theta) - \mathbf{a}(\theta)\|^2. \quad (73)$$

Notice that the first quantity of $h(\theta)$ is nothing other than the MUSIC cost function, while the k^{th} term of the second quantity is the residual after projecting onto the null-space defined through $\widehat{\mathbf{Q}}_k^\perp$. Now that we have an estimated value of $\widehat{\boldsymbol{\Theta}}^{\text{tar}}$, we can update the orthogonal projector $\widehat{\mathbf{P}}_0^\perp$ as follow

$$\widehat{\mathbf{P}}_0^\perp = \mathbf{I}_N - \mathbf{A}(\widehat{\boldsymbol{\Theta}}^{\text{tar}}) (\mathbf{A}^H(\widehat{\boldsymbol{\Theta}}^{\text{tar}}) \mathbf{A}(\widehat{\boldsymbol{\Theta}}^{\text{tar}}))^{-1} \mathbf{A}^H(\widehat{\boldsymbol{\Theta}}^{\text{tar}}). \quad (74)$$

Finally, we go back to the first phase of the method and repeat until convergence of $\widehat{\boldsymbol{\Theta}}^{\text{tar}}$ and $\widehat{\boldsymbol{\Theta}}^{\text{u}}$. A summary of the proposed method is given in **Algorithm 2**.

Algorithm 2 Alternating "Project-then-Fuse" Subspace Estimation

```

INPUT:  $\widehat{\mathbf{R}}_0 \dots \widehat{\mathbf{R}}_K$ 
INITIALIZE:
0.1) Obtain the noise subspace of the DL covariance  $\widehat{\mathbf{U}}_{N,0}$ 
    by EVD on  $\widehat{\mathbf{R}}_0$  as in (40).
0.2) Compute  $\widehat{\mathbf{P}}_0^\perp \leftarrow \mathbf{I}_N - \widehat{\mathbf{U}}_{N,0} \widehat{\mathbf{U}}_{N,0}^H$ 
# PHASE 1: Project then estimate.
FOR  $k = 1 \dots K$ 
    1.1) Obtain  $\widehat{\mathbf{R}}_k$  via (45).
    1.2) Extract  $\mathbf{v}_{S,k}$  via SVD as shown in (43).
    1.3) Obtain  $\hat{\theta}_{k,u}^{\text{u}}$  by maximizing (56).
    1.4) Update  $\widehat{\boldsymbol{\Theta}}_k \leftarrow \hat{\theta}_{k,u}^{\text{u}}$ .
    1.5) Compute  $\widehat{\mathbf{Q}}_k^\perp$ , given  $\hat{\theta}_{k,u}^{\text{u}}$  via (57).
    1.6) Compute  $\widehat{\mathbf{S}}_k$  following (58).
    1.7) Extract  $\widehat{\mathbf{V}}_{S,k}$  through SVD as in (59).
# PHASE 2: Fuse then estimate.
2.1) Obtain  $\widehat{\boldsymbol{\Theta}}^{\text{tar}}$  by finding the  $q$  strongest peaks in  $h^{-1}(\theta)$ 
    as shown in (72).
2.2) Update  $\widehat{\mathbf{P}}_0^\perp$  using the most recent estimates of  $\widehat{\boldsymbol{\Theta}}^{\text{tar}}$  as
 $\widehat{\mathbf{P}}_0^\perp = \mathbf{I}_N - \mathbf{A}(\widehat{\boldsymbol{\Theta}}^{\text{tar}}) (\mathbf{A}^H(\widehat{\boldsymbol{\Theta}}^{\text{tar}}) \mathbf{A}(\widehat{\boldsymbol{\Theta}}^{\text{tar}}))^{-1} \mathbf{A}^H(\widehat{\boldsymbol{\Theta}}^{\text{tar}})$ .
2.3) Go back to Phase 1.
return  $\widehat{\boldsymbol{\Theta}}^{\text{tar}}, \widehat{\boldsymbol{\Theta}}^{\text{u}}$ 
    
```

VI. SIMULATION RESULTS

A. Parameter Setup

Assume that both the transmit and receive antenna arrays are equipped with N antennas and follow a uniform linear antenna

(ULA) configuration spaced at half a wavelength, i.e. $\frac{\lambda}{2}$. The carrier frequency is set at $f_c = 24\text{GHz}$. For OFDM transmissions, the subcarrier spacing is set to $\Delta_f = 240\text{kHz}$; hence, the symbol duration is $T = \frac{1}{\Delta_f} = 4.1667\mu\text{sec}$. The cyclic prefix duration is set to $T_{\text{CP}} = \frac{T}{4} = 1.0417\mu\text{sec}$. Therefore, the total symbol duration is equal to $T_o = T + T_{\text{CP}} = 5.2084\mu\text{sec}$. The constellation used is a quadrature phase shift keying (QPSK). Communication users are assumed to be located at equidistant angles, namely, the k^{th} user is located at $\theta_k^{\text{u}} = [-10 - (k-1)\frac{60}{K-1}]^\circ$. All users are considered to be in LoS with the DFRC BS. Monte Carlo type experiments are conducted herein, where each trial generates an independent channel realization. The number of Monte Carlo simulations is set to 10^4 trials. The MSE is computed as follows

$$\text{MSE} = \frac{1}{qE} \sum_{e=1}^E \sum_{p=1}^q (\hat{\theta}_p^{\text{tar}}(e) - \theta_k)^2, \quad (75)$$

where $\hat{\theta}_p^{\text{tar}}(e)$ is the estimate of the p^{th} target in the e^{th} Monte Carlo experiment, and E is the total number of experiments. All other parameters are mentioned in Section VI-D.

B. Benchmark Schemes

For the sake of performance comparisons, we include the following benchmarks in our performance study:

a) *Naive MUSIC*: We coin the term "Naive MUSIC", as the method which simply averages all the covariance matrices at hand to form a single covariance matrix $\widehat{\mathbf{R}} = \frac{1}{K} \sum_{k=1}^K \widehat{\mathbf{R}}_k$. This step is followed by an eigenvalue decomposition to extract the signal and noise subspaces in order to compute the MUSIC criterion.

b) *Algorithm 1 with prior knowledge of user AoAs*: This benchmark runs Algorithm 1 under the condition that the true user AoAs are fed to the algorithm. More specifically, the first phase of Algorithm 1 is then unnecessary, and is therefore bypassed, because $\hat{\theta}_k^{\text{u}}$ are replaced by θ_k^{u} , for all $k = 1 \dots K$.

c) *CRB*: The CRB is a benchmark giving the lower bound on the variance of any unbiased estimator of a deterministic parameter. Following the model introduced in Section II, the CRB of the target AoAs [49] can be shown to be

$$\text{CRB}(\boldsymbol{\Theta}^{\text{tar}}) = \frac{\sigma^2}{2} \left(\sum_{k=0}^K \sum_{\ell=0}^{\bar{L}_k} \mathbf{S}_k \mathbf{F}_{k,\ell} \mathbf{S}_k^T \right)^{-1}, \quad (76)$$

where

$$\mathbf{F}_{k,\ell} = \text{Re}\{\text{diag}(\mathbf{X}_k(:,\ell))^* \mathbf{H}_k \text{diag}(\mathbf{X}_k(:,\ell))\}, \quad (77)$$

$$\mathbf{H}_k = \mathbf{D}_k^H (\mathbf{I} - \mathbf{P}_k) \mathbf{D}_k. \quad (78)$$

The expression of \mathbf{P}_k is given in (26), \mathbf{D}_k is the derivative of the manifold matrix given in (18), and \mathbf{S}_k is a selection matrix indexing the columns of the common manifold matrix, $\mathbf{A}(\boldsymbol{\Theta}^{\text{tar}})$. Furthermore, the CRB of the mono-static and the bi-static cases (for $K = 1$) are also illustrated to show the advantage of the hybrid scheme.

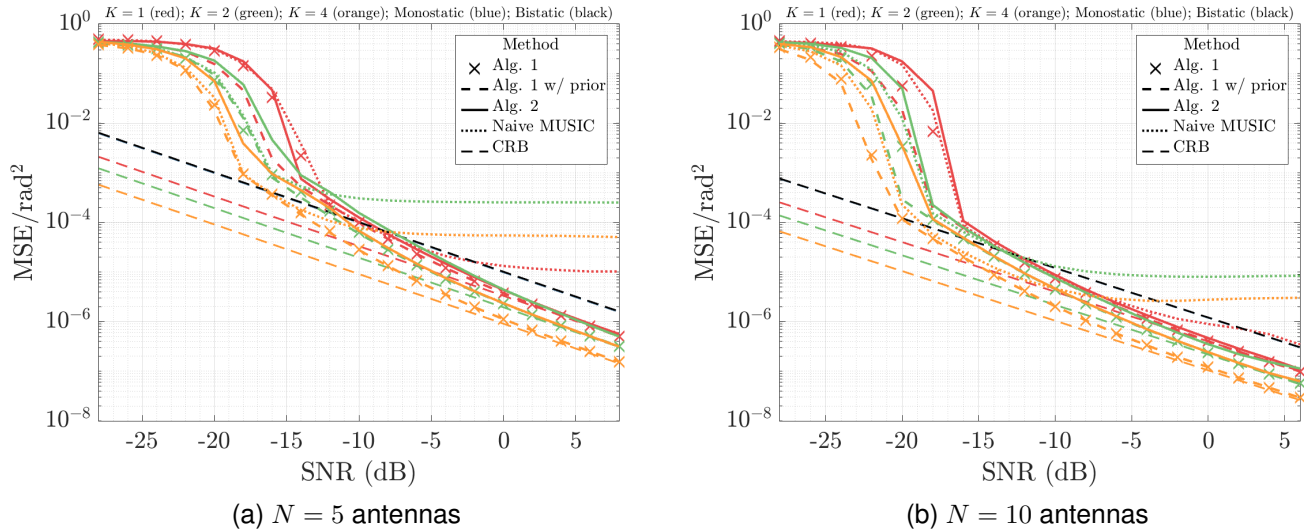


Fig. 2. Scenario 1: The MSE versus SNR of the proposed methods and benchmarks for different number of communication users and $q = 1$ target located at 0° .

C. Scenarios

We distinguish between two scenarios:

- Scenario 1: In this scenario, the product of the number of subcarriers and the number of OFDM symbols are set to be equal. In other words, for any K users, the factor $L_k|\mathcal{C}_k|$ is held constant for all k . The aim of studying this scheme is to show the performance of time-frequency resource fairness and its impact on the MSE of the estimated AoAs via the different methods described in this article. More precisely, if K users are participating in the UL, the k^{th} user is allocated $|\mathcal{C}_k| = \frac{32}{K}$ subcarriers, and $L_k = 16K$ OFDM symbols.
- Scenario 2: In this scenario, we fix the number of OFDM symbols to $L_k = 32$ for each communication users and allocate $|\mathcal{C}_k| = 32$ subcarriers for each user. In other words, more communication users participating in the UL requires more bandwidth.

D. Simulation Results

a) Scenario 1 with a single target: In Fig. 2, we plot the MSE of the estimated AoAs as a function of varying SNR, for different number of antennas. In Fig. 2a, we fix $N = 5$ antennas and $q = 1$ target located at $\theta_1^{\text{tar}} = 0^\circ$. We see that Algorithm 1 with AoA prior achieves the best performance for any K as compared to other methods, which is caused by less unknown parameters being estimated than other presented methods. Interestingly, as K increases, Algorithm 1 without the user AoA prior knowledge coincides with that with prior information. Moreover, both versions of Algorithm 1 achieve the CRB starting at an SNR of 2 dB. On the other hand, for an MSE accuracy of 10^{-4} , Algorithm 2 loses about 4 dB in SNR as compared to Algorithm 1, and outperforms the Naive MUSIC benchmark, even at high SNR. When more communication users are participating in the UL, we see that doubling the number of users contributes to an overall MSE

improvement of about 3.2 dB. This can be explained through time diversity, i.e. the participation of more users within the same bandwidth, but through the availability of more OFDM symbols. In Fig. 2b, we fix $N = 10$ antennas, as well as $q = 1$ target with $\theta_1^{\text{tar}} = 0^\circ$. We can notice that both versions of Algorithm 1 achieve the CRB for all K , with an improved performance over that in Fig. 2a due to an increase in number of antennas. Moreover, as more communication users participate in the UL, the performance of both versions of Algorithm 1 approaches its CRB faster. This is due to the participation of more users in the UL over the same bandwidth resource. For instance, at SNR = -20 dB, Algorithm 1 is only 0.0017 rad^2 far away from its CRB for $K = 4$, and 0.18 rad^2 for $K = 1$. Moreover, we see that for increasing K , Algorithm 1 approaches the version of itself with prior user AoAs, which is explained through time diversity, i.e. when more OFDM symbols are available at the disposal of the DFRC BS, a better MSE performance is expected, in general. In particular, for an accuracy of 10^{-3} , and for $K = 1$, the gap between both versions of Algorithm 1 is 1.2 dB, compared to 1 dB for $K = 2$, and 0.7 dB for $K = 4$. Moreover, Algorithm 2 generally performs better than the Naive MUSIC benchmark in the high SNR regime. For example, at $K = 2$, the performance of Algorithm 2 begins to outperform the Naive MUSIC benchmark starting from SNR = -11 dB, and SNR = -7 dB for $K = 8$, which can also be explained through more users transmitting in the UL, thus providing more OFDM samples towards the DFRC BS. Also, notice that the CRB of the mono-static and bi-static configurations coincide.

b) Scenario 1 with multiple targets: In Fig. 3, we follow the same scenario as in Fig. 2, but this time tripling the number of targets, i.e. $q = 3$. The targets are assumed to be located at $0^\circ, 30^\circ, 60^\circ$, respectively. This study will show the improvements of MSE estimates with an increasing number of communication users, even with more targets. The number

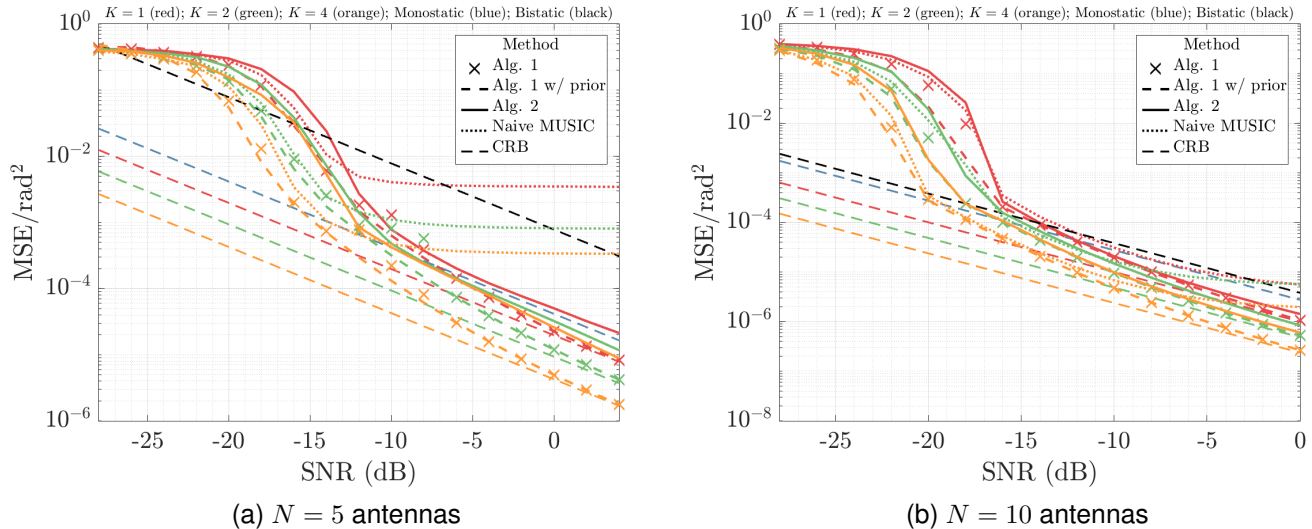


Fig. 3. Scenario 1: The MSE versus SNR of the proposed methods and benchmarks for a different number of communication users and $q = 3$ targets located at $0^\circ, 30^\circ, 60^\circ$.

of subcarriers and OFDM symbols for the k^{th} user is also the same as that in Fig. 2. Note that the case of $K = 0$ refers to the *mono-static only* case, where only the echo received due to the DL signal is used at the DFRC BS. In Fig. 3a, we fix $N = 5$ antennas. As was previously the case, we can observe that the benchmark of Algorithm 1 with AoA prior achieves the best performance for a different number of communication users. The improvement of performance with increasing communication users is still preserved, as we see a factor of 3 dB gain in CRB, when doubling K . Nevertheless, both versions of Algorithm 1 achieve the CRB starting at SNR = 0 dB. Moreover, we see that Algorithm 2 generally outperforms the Naive MUSIC benchmark starting from SNR = -11 dB for $K = 1$, SNR = -10 dB for $K = 8$ users, which can also be explained by the availability of more time resources, which becomes more notable for a higher number of communication users. In Fig. 3b, we fix $N = 10$ antennas, as well as $q = 3$ targets. We can also say that the gap between both versions of Algorithm 1 shrinks with increasing K . For instance, both versions coincide at an accuracy of 10^{-2} and for $K = 16$ users, as compared to a 0.5 dB gap for $K = 1$ communication users. The Naive MUSIC benchmark also approaches the CRB for higher N , but saturates after SNR = 4 dB for $K = 1, 2$. This loss of performance in Naive MUSIC is due to the fact that the method does not exploit the common manifold and, so, treats all AoAs, whether targets or users, equally.

c) Scenario 2 with a single target: In Fig. 4, we switch to Scenario 2, where we plot the MSE of the estimated AoAs as a function of varying SNR, for different number of antennas. As done previously, we study the performance for $N = 5$ and $N = 10$ antennas. In Fig. 4a, we fix $N = 5$ antennas for a single target located at 0° . As is the case in previous experiments, both versions of Algorithm 1 coincide and meet the CRB, however, the MSE of Naive MUSIC saturates

with increasing SNR. For instance, focusing on $K = 2$, we can see that at SNR = -14 dB, the MSE curve of Naive MUSIC begins to saturate, whereas the MSE of Algorithm 2 approaches the CRB with an increase of SNR. This is explained through Algorithm 2's effectiveness in segregating the common manifold. A similar observation is given for all other values of K . In Fig. 4b, we fix $N = 10$ antennas with a single source as in Fig. 4a. We can also report that both versions of Algorithm 1 converge towards the CRB at high SNR. Furthermore, for an MSE level of 10^{-4} rad², there is a 0.4 dB gain when doubling the number of users from $K = 1$ to $K = 2$, followed by a gain of 0.6 dB between $K = 2$ and $K = 4$. This gain is explained through the availability of more bandwidth, where as we increase the number of communication users, we also increase the bandwidth to accommodate the users. Furthermore, each user will provide a better spatial view of the target through its UL contribution.

d) Scenario 2 with multiple targets: In Fig. 5, we follow the same scenario as that in Fig. 4, but we place $q = 3$ targets, instead of $q = 1$. As is the case in Fig. 3, the targets are assumed to be located at $0^\circ, 30^\circ, 60^\circ$, respectively. We aim to study the performance with multiple targets. In Fig. 5a, we fix $N = 5$ antennas and $q = 3$ targets. We observe that both versions of Algorithm 1 coincide with the CRB as the SNR increases. Observe that, in general, Naive MUSIC saturates earlier than the case of $q = 1$ targets, i.e. compared to Fig. 4a. For example, at $K = 1$, the Naive MUSIC begins to saturate at SNR = -10 dB at an MSE level of about 0.003 rad², as compared to Fig. 4a as compared to 10^{-5} rad² at SNR = 0 dB. This goes ahead to show that Naive MUSIC is expected to do worse for more targets, due to its inability to distinguish the common target manifold. In contrast, Algorithm 2 approaches the CRB for high SNR. In Fig. 5b, we fix $N = 10$ antennas and $q = 3$ targets. Again, we observe that both versions of Algorithm 1 converge to the CRB

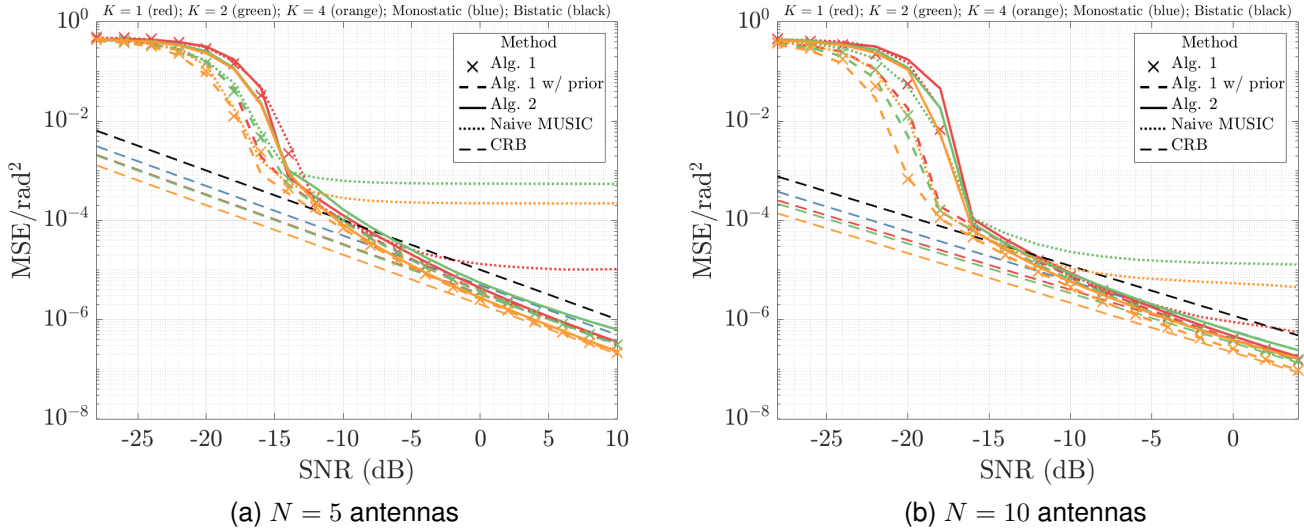


Fig. 4. Scenario 2: The MSE versus SNR of the proposed methods and benchmarks for different number of communication users and $q = 1$ target located at 0° .

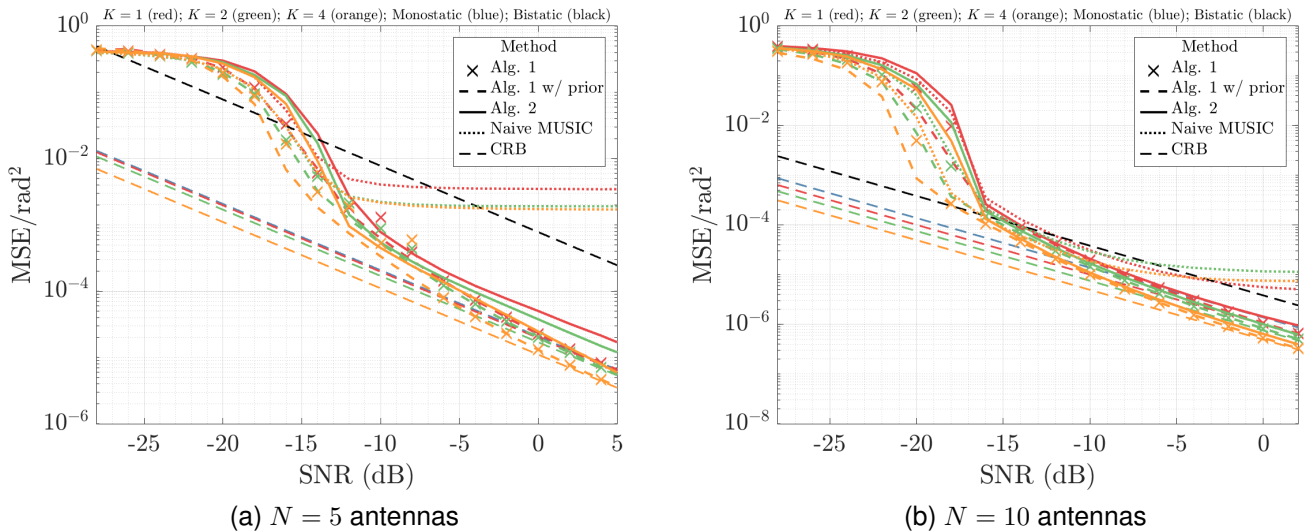


Fig. 5. Scenario 2: The MSE versus SNR of the proposed methods and benchmarks for a different number of communication users and $q = 3$ targets located at $0^\circ, 30^\circ, 60^\circ$.

at high SNR, whereas the Naive MUSIC saturates. Algorithm 2 decays with the CRB for high SNR. We also see gains for Algorithm 2, when compared to Naive MUSIC algorithm. For example, at an MSE level of 10^{-5} rad^2 and at $K = 1$, we see that Algorithm 2 gains about 2.5 dB compared to Naive MUSIC and a 5 dB gain for $K = 4$.

e) AoA Behavior: In Fig. 6, we seek to study the estimated AoA behavior of the proposed methods as a function of iteration number. The estimate of each target AoA at any given iteration is averaged over Monte Carlo trials. The chosen SNR is -12 dB and the number of antennas is set to $N = 5$ and $K = 16$ communication users. We observe that all three methods converge even at low SNR. Even more, when the user AoAs are fed as prior information into Algorithm 1, we can see a slight faster convergence than the case without

the prior information, most notably around the 3^{rd} iteration in an attempt to estimate $\theta_3^{\text{tar}} = 60^\circ$. Furthermore, all methods converge after 5 number of iterations. This proves the effectiveness and stability of all the proposed methods, from a convergence viewpoint, even at low SNR.

f) Spectra Comparison: In Fig. 7, we reveal some internal dynamics of Algorithm 2, namely the spectrum $h^{-1}(\theta)$, where its maximization is involved within the second phase of Algorithm 2. Therefore, a reasonable comparison of spectra would be $h^{-1}(\theta)$, compared to the classical MUSIC spectrum. Furthermore, the spectra of each method have been averaged over Monte Carlo trials. Herein, we fix SNR = 10 dB, $K = 16$ users, $q = 3$ targets located at $0^\circ, 30^\circ, 60^\circ$ and $N = 5$ antennas. Not only can we notice an accurate estimation of the true target AoAs, but we can also report sharper peaks

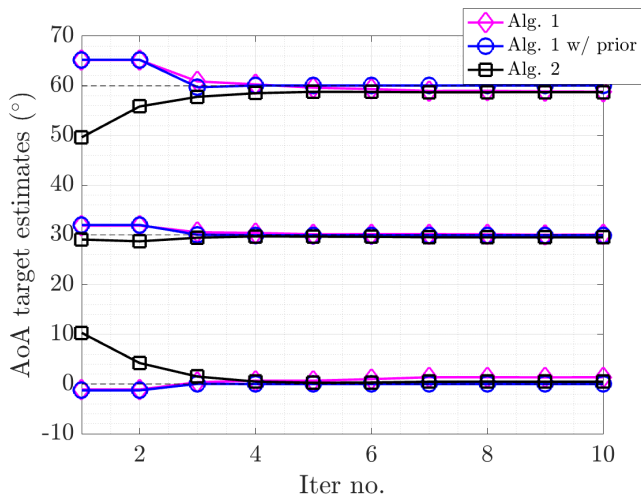


Fig. 6. The behavior of the different algorithms as a function of iteration number.

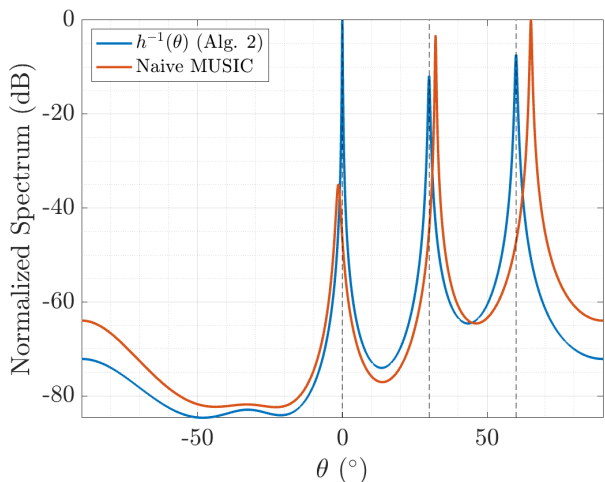


Fig. 7. A spectrum comparison of $h^{-1}(\theta)$ given in Algorithm 2 vs. the MUSIC spectrum. The vertical dashed lines correspond to the true target AoAs.

and an improved resolution, as compared to the Naive MUSIC one, which further allows for better target AoA estimation. Moreover, notice that the noise level of the spectra has been reduced by more than 6 dB, especially around the region $[-70^\circ, -50^\circ]$. This again proves superiority of Algorithm 2, when compared to the MUSIC estimator.

g) Behavior of $g(\theta)$: In Fig. 8, we further highlight additional dynamics of Algorithm 2, namely the spectrum $g_k^{-1}(\theta)$, found in the first phase of Algorithm 2. As a reminder, the k^{th} spectrum, $g_k^{-1}(\theta)$, aids in identifying the AoA of the k^{th} user. As is the case of Fig. 7, each spectrum is averaged over different Monte Carlo trials. The SNR is set to 10 dB, the number of users is set to $K = 16$, and the number of antennas is set to $N = 5$ antennas. First, we can see one and only one peak for any $g_k^{-1}(\theta)$. This is a good indicator, as $g_k^{-1}(\theta)$ should be highly selective of its associated user (i.e. the k^{th} user) and also capable of simultaneously rejecting off all other users and targets, even with a low number of antennas

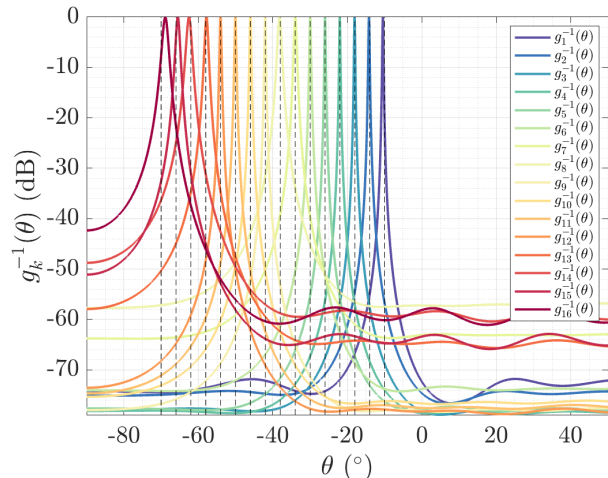


Fig. 8. The different spectra, i.e. $g_1^{-1}(\theta) \dots g_{K}^{-1}(\theta)$, involved in the first phase of Algorithm 2. The vertical dashed lines correspond to the true user AoAs.

i.e., $N = 5$. With this feature in mind, we see that there are no spurious peaks arising in any of the spectra. Moreover, we can observe that the peaks sharpen, as the user approaches broad-fire of the antenna array. Furthermore, we also notice that the noise levels decrease as the user approaches the end-fire of the antenna array, which is a typical characteristic of ULA.

VII. CONCLUSIONS AND OUTLOOK

In this paper, a new hybrid radar model is proposed, where the DFRC BS acts as a mono-static radar in the DL and the communication users act as distributed bi-static radars in the UL, following an FDD protocol. From the DFRC BS perspective, we derive the ML criterion of the AoA estimation problem, and assemble its connections with the classical AoA estimation problem. We take a step further in proposing two efficient estimators. The first algorithm is built on the direct optimization of the FML criterion by alternating between the user and target terms in the ML cost function. Furthermore, the second algorithm diligently forms an iterative procedure through the formulation of suitable optimization methods that exploit the common manifold structure appearing over different communication bands. Our simulation findings prove the effectiveness of the proposed hybrid radar model, along with the methods involved in resolving and estimating the locations. In short, the proposed communication-centric hybrid radar model has proven its potential and superiority in improving target location estimates in different communication settings.

Research directions include extensions toward wide-band scenarios, which further lead to frequency-dependent array response vectors. In addition, due to full duplex operation, we plan to propose estimators, as well as compensators, for the self-interference leakage phenomenon caused by the transmitting onto the receiving unit of the DFRC BS. Another direction is the multi-parameter estimation case, where the ToA and Doppler parameters are to be jointly estimated with the directions of arrival. The introduced hybrid radar model

can be extended to accommodate large network scenarios. Moreover, from an estimation perspective, we also allude to the need for more sophisticated algorithms that can trade complexity for performance, and vice-versa.

REFERENCES

- [1] J. A. Zhang *et al.*, “Enabling Joint Communication and Radar Sensing in Mobile Networks—A Survey,” *IEEE Communications Surveys & Tutorials*, vol. 24, no. 1, pp. 306–345, 2022.
- [2] F. Liu *et al.*, “Joint Radar and Communication Design: Applications, State-of-the-Art, and the Road Ahead,” *IEEE Transactions on Communications*, vol. 68, no. 6, pp. 3834–3862, 2020.
- [3] K. V. Mishra *et al.*, “Toward Millimeter-Wave Joint Radar Communications: A Signal Processing Perspective,” *IEEE Signal Processing Magazine*, vol. 36, no. 5, pp. 100–114, 2019.
- [4] A. Liu *et al.*, “A Survey on Fundamental Limits of Integrated Sensing and Communication,” *IEEE Communications Surveys & Tutorials*, vol. 24, no. 2, pp. 994–1034, 2022.
- [5] M. Chaffii *et al.*, “Twelve Scientific Challenges for 6G: Rethinking the Foundations of Communications Theory,” *IEEE Communications Surveys & Tutorials*, pp. 1–1, 2023.
- [6] J. Choi *et al.*, “Millimeter-Wave Vehicular Communication to Support Massive Automotive Sensing,” *IEEE Communications Magazine*, vol. 54, no. 12, pp. 160–167, 2016.
- [7] J. Yu *et al.*, “6G mobile-edge empowered metaverse: Requirements, technologies, challenges and research directions,” *arXiv preprint arXiv:2211.04854*, 2022.
- [8] U. Demirhan and A. Alkhateeb, “Integrated sensing and communication for 6G: Ten key machine learning roles,” *arXiv preprint arXiv:2208.02157*, 2022.
- [9] X. Cheng *et al.*, “Integrated Sensing and Communications (ISAC) for Vehicular Communication Networks (VCN),” *IEEE Internet of Things Journal*, vol. 9, no. 23, pp. 23 441–23 451, 2022.
- [10] Z. Wang *et al.*, “NOMA Empowered Integrated Sensing and Communication,” *IEEE Communications Letters*, vol. 26, no. 3, pp. 677–681, 2022.
- [11] X. Mu *et al.*, “NOMA for Integrating Sensing and Communications towards 6G: A Multiple Access Perspective,” *IEEE Wireless Communications*, pp. 1–8, 2023.
- [12] H. Zhang *et al.*, “Holographic Integrated Sensing and Communication,” *IEEE Journal on Selected Areas in Communications*, vol. 40, no. 7, pp. 2114–2130, 2022.
- [13] H. He *et al.*, “Integrated sensing and communication in an optical fibre,” *Light: Science & Applications*, vol. 12, no. 1, p. 25, 2023.
- [14] F. Liu *et al.*, “Integrated sensing and communications: Toward dual-functional wireless networks for 6g and beyond,” *IEEE Journal on Selected Areas in Communications*, vol. 40, no. 6, pp. 1728–1767, 2022.
- [15] X. Song *et al.*, “Joint Transmit and Reflective Beamforming for IRS-Assisted Integrated Sensing and Communication,” in *2022 IEEE Wireless Communications and Networking Conference (WCNC)*, 2022, pp. 189–194.
- [16] Z. Xiao and Y. Zeng, “Waveform Design and Performance Analysis for Full-Duplex Integrated Sensing and Communication,” *IEEE Journal on Selected Areas in Communications*, vol. 40, no. 6, pp. 1823–1837, 2022.
- [17] J. Mu *et al.*, “UAV Meets Integrated Sensing and Communication: Challenges and Future Directions,” *IEEE Communications Magazine*, pp. 1–7, 2022.
- [18] A. Bazzi and M. Chaffii, “On Outage-based Beamforming Design for Dual-Functional Radar-Communication 6G Systems,” *IEEE Transactions on Wireless Communications*, pp. 1–1, 2023.
- [19] Q. Qi *et al.*, “Integrated Sensing, Computation and Communication in B5G Cellular Internet of Things,” *IEEE Transactions on Wireless Communications*, vol. 20, no. 1, pp. 332–344, 2021.
- [20] J. A. Zhang *et al.*, “An Overview of Signal Processing Techniques for Joint Communication and Radar Sensing,” *IEEE Journal of Selected Topics in Signal Processing*, vol. 15, no. 6, pp. 1295–1315, 2021.
- [21] R. M. Mealey, “A Method for Calculating Error Probabilities in a Radar Communication System,” *IEEE Transactions on Space Electronics and Telemetry*, vol. 9, no. 2, pp. 37–42, 1963.
- [22] A. Bazzi and M. Chaffii, “On Integrated Sensing and Communication Waveforms with Tunable PAPR,” *arXiv preprint arXiv:2210.02892*, 2022.
- [23] A. Hassanien *et al.*, “Dual-Function Radar-Communications: Information Embedding Using Sidelobe Control and Waveform Diversity,” *IEEE Transactions on Signal Processing*, vol. 64, no. 8, pp. 2168–2181, 2016.
- [24] M. Nowak *et al.*, “Co-designed radar-communication using linear frequency modulation waveform,” *IEEE Aerospace and Electronic Systems Magazine*, vol. 31, no. 10, pp. 28–35, 2016.
- [25] T. Huang *et al.*, “MAJoRCom: A Dual-Function Radar Communication System Using Index Modulation,” *IEEE Transactions on Signal Processing*, vol. 68, pp. 3423–3438, 2020.
- [26] M. Temiz *et al.*, “An Experimental Study of Radar-Centric Transmission for Integrated Sensing and Communications,” *IEEE Transactions on Microwave Theory and Techniques*, pp. 1–14, 2023.
- [27] A. Hassanien *et al.*, “Signaling strategies for dual-function radar communications: an overview,” *IEEE Aerospace and Electronic Systems Magazine*, vol. 31, no. 10, pp. 36–45, 2016.
- [28] A. Bazzi and M. Chaffii, “RIS-Enabled Passive Radar towards Target Localization,” *arXiv preprint arXiv:2210.11887*, 2022.
- [29] L. Gaudio *et al.*, “On the Effectiveness of OTFS for Joint Radar Parameter Estimation and Communication,” *IEEE Transactions on Wireless Communications*, vol. 19, no. 9, pp. 5951–5965, 2020.
- [30] A. Hassanien *et al.*, “Dual-Function Radar Communication Systems: A Solution to the Spectrum Congestion Problem,” *IEEE Signal Processing Magazine*, vol. 36, no. 5, pp. 115–126, 2019.
- [31] Y. Yang *et al.*, “Omnidirectional Motion Classification With Monostatic Radar System Using Micro-Doppler Signatures,” *IEEE Transactions on Geoscience and Remote Sensing*, vol. 58, no. 5, pp. 3574–3587, 2020.
- [32] F. Colone *et al.*, “A Multistage Processing Algorithm for Disturbance Removal and Target Detection in Passive Bistatic Radar,” *IEEE Transactions on Aerospace and Electronic Systems*, vol. 45, no. 2, pp. 698–722, 2009.
- [33] M. S. Greco *et al.*, “Cramer-Rao Bounds and Selection of Bistatic Channels for Multistatic Radar Systems,” *IEEE Transactions on Aerospace and Electronic Systems*, vol. 47, no. 4, pp. 2934–2948, 2011.
- [34] H. Kuschel *et al.*, “Deployable multiband passive/active radar for air defense (DMPAR),” *IEEE Aerospace and Electronic Systems Magazine*, vol. 28, no. 9, pp. 37–45, 2013.
- [35] F. Wang and H. Li, “Joint Waveform and Receiver Design for Co-Channel Hybrid Active-Passive Sensing With Timing Uncertainty,” *IEEE Transactions on Signal Processing*, vol. 68, pp. 466–477, 2020.
- [36] S. D. Liyanaarachchi *et al.*, “Optimized Waveforms for 5G–6G Communication With Sensing: Theory, Simulations and Experiments,” *IEEE Transactions on Wireless Communications*, vol. 20, no. 12, pp. 8301–8315, 2021.
- [37] L. Leyva *et al.*, “Two-stage estimation algorithm based on interleaved OFDM for a cooperative bistatic ISAC scenario,” in *2022 IEEE 95th Vehicular Technology Conference: (VTC2022-Spring)*, 2022, pp. 1–6.
- [38] Z. Yu *et al.*, “Location Sensing and Beamforming Design for IRS-Enabled Multi-User ISAC Systems,” *IEEE Transactions on Signal Processing*, vol. 70, pp. 5178–5193, 2022.
- [39] R. Hadani *et al.*, “Orthogonal Time Frequency Space Modulation,” in *2017 IEEE Wireless Communications and Networking Conference (WCNC)*, 2017, pp. 1–6.
- [40] R. Bomfim *et al.*, “Channel estimation for MIMO space time coded OTFS under doubly selective channels,” in *2021 IEEE International Conference on Communications Workshops (ICC Workshops)*. IEEE, 2021, pp. 1–6.
- [41] W. Yuan *et al.*, “Integrated Sensing and Communication-Assisted Orthogonal Time Frequency Space Transmission for Vehicular Networks,” *IEEE Journal of Selected Topics in Signal Processing*, vol. 15, no. 6, pp. 1515–1528, 2021.
- [42] L. Pucci *et al.*, “System-Level Analysis of Joint Sensing and Communication Based on 5G New Radio,” *IEEE Journal on Selected Areas in Communications*, vol. 40, no. 7, pp. 2043–2055, 2022.
- [43] F. Liu *et al.*, “Toward Dual-functional Radar-Communication Systems: Optimal Waveform Design,” *IEEE Transactions on Signal Processing*, vol. 66, no. 16, pp. 4264–4279, 2018.
- [44] N. Su *et al.*, “Sensing-Assisted Eavesdropper Estimation: An ISAC Breakthrough in Physical Layer Security,” *arXiv preprint arXiv:2210.08286*, 2022.
- [45] C. R. Rao *et al.*, “Linear models and generalizations,” *Least Squares and Alternatives (3rd edition)* Springer, Berlin Heidelberg New York, 2008.
- [46] I. Ziskind and M. Wax, “Maximum likelihood localization of multiple sources by alternating projection,” *IEEE Transactions on Acoustics, Speech, and Signal Processing*, vol. 36, no. 10, pp. 1553–1560, 1988.
- [47] A. Bazzi and D. Slock, “Robust Music Estimation Under Array Response Uncertainty,” in *ICASSP 2020 - 2020 IEEE International Conference on Acoustics, Speech and Signal Processing (ICASSP)*, 2020, pp. 4821–4825.
- [48] K. B. Petersen *et al.*, “The matrix cookbook,” *Technical University of Denmark*, vol. 7, no. 15, p. 510, 2008.

- [49] P. Stoica and A. Nehorai, "MUSIC, maximum likelihood, and Cramer-Rao bound," *IEEE Transactions on Acoustics, Speech, and Signal Processing*, vol. 37, no. 5, pp. 720–741, 1989.